regulation of these receptors amplifies the release of PGE_2, with subsequent formation of cAMP, leading the inhibition of LPS-induced TNF-α release (Caggiano and Kraig, 1999; Webb et al., 2003). PGE_2 and cAMP were suggested to be neuroprotective (Kim et al., 2002), while COX enzymes and prostanoids are reported to mediate both neurodegeneration and neuroprotection during brain inflammation (Tzeng et al., 2005) and lack of a microglial EP_2 receptor protected against the neurotoxic effects of the cerebral innate immune response (Shie et al., 2005).

Protective effects of BK

In the CNS, microglia are the major cell population responding to LPS and this activation is mediated via a Toll-like receptor 4 (TLR4)-dependent pathway (Lehnardt et al., 2003). The BK-induced inhibition of LPS-induced TNF-α release could be protective for neurons suffering from the toxic effect of TNF-α and IL-1β. LPS-induced neuronal apoptotic cell death through the intracellular cAMP system is associated with the modulation of NO from microglial cells and reactive oxygen species (ROS) production from neurons (Kim et al., 2002). BK has anti-inflammatory effects due to its attenuation of the release of pro-inflammatory cytokines such as TNF-α and IL-1β from the microglia, and this may mediate neuroprotection. This is in contrast to the general concept of kinins as mediators of inflammatory diseases and pain, because beneficial effects of B_2 receptor antagonists have been reported (Heitsch, 2000). Furthermore, activation of neuronal B_2 receptor produces pain hypersensitivity by potentiating glutamatergic transmission (Wang et al., 2005) and induces glutamate release from astrocytes (Parpura et al., 1994). Therefore, effects of BK in microglia might be distinct from those in other cell types in the CNS.

The multiple effects of BK via microglia are summarized in Figure 1. Microglia migrate to the lesion site, react to BK, and release NO and PGE_2. In response to a lesion, BK and the expression of its receptors are up-regulated in microglia, thereby amplifying the release of PGE_2. The released PGE_2 interacts with microglial EP_2 and EP_4 receptors (which are also up-regulated by BK), increases intracellular cAMP, and down-regulates the release of TNF-α and IL-1β. The role of BK-induced NO release has not yet been elucidated, but presumably competes with the contraction of blood vessels after the lesion (Nimmerjahn et al., 2005) by amplifying the vasodilation induced by B_2 receptor-hyperpolariztion and NO-cGMP signaling (Frieden et al., 1999; Miura et al., 1999; Batenburg et al., 2005).

In conclusion, BK is a candidate important signal in brain injury. There are many neuropeptides that are elevated following neural injury and have putative roles in glia (Ubink et al., 2003). In particular, galanin has an inhibitory effect on micrgolial TNF-α production (Su et al., 2003) similar to that of BK. These results strongly indicate that BK deserves attention as a member of the family of neuropeptides, as already proposed by Hallberg and Nyberg (2003), and its protective role could be valuable for the treatment of neuropathic pain, lesion, or inflammation.

Acknowledgments

This work was supported by Grants-in-Aid for Scientific Research from the Japan Society for the Promotion of Science and from the Ministry of Health, Labor and Welfare, Japan.

References

Abbott, N.J. (2000). Inflammatory mediators and modulation of blood-brain barrier permeability. Cell Mol. Neurobiol. *20*, 131–147.

Batenburg, W.W., Tom, B., Schuijt, M.P., and Danser, A.H. (2005). Angiotensin II type 2 receptor-mediated vasodilation. Focus on bradykinin, NO and endothelium-derived hyperpolarizing factor(s). Vascul. Pharmacol. *42*, 109–118.

Bernstein, M., Lyons, S.A., Moller, T., and Kettenmann, H. (1996). Receptor-mediated calcium signalling in glial cells from mouse corpus callosum slices. J. Neurosci. Res. *46*, 152–163.

Burch, R.M. and Kniss, D.A. (1988). Modulation of receptor-mediated signal transduction by diacylglycerol mimetics in astrocytes. Cell Mol. Neurobiol. *8*, 251–257.

Caggiano, A.O. and Kraig, R.P. (1999). Prostaglandin E receptor subtypes in cultured rat microglia and their role in reducing lipopolysaccharide-induced interleukin-1β production. J. Neurochem. *72*, 565–575.

Chandy, K.G., Wulff, H., Beeton, C., Pennington, M., Gutman, G., and Cahalan, M.D. (2004). K^+ channels as targets for specific immunomodulation. Trends. Pharmacol. Sci. *25*, 280–289.

Chao, J., Chao, L., Swain, C.C., Tsai, J., and Margolius, H.S. (1987). Tissue kallikrein in rat brain and pituitary: regional distribution and estrogen induction in the anterior pituitary. Endocrinology *120*, 475–482.

Davalos, D., Grutzendler, J., Yang, G., Kim, J.V., Zuo, Y., Jung, S., Littman, D.R., Dustin, M.L., and Gan, W.B. (2005). ATP mediates rapid microglial response to local brain injury *in vivo*. Nat. Neurosci. *8*, 752–758.

Delmas, P., Wananerbercq, N., Abogadie, F.C., Mistry, M., and Brown, D.A. (2002). Signaling microdomains define the specificity of receptor-mediated $InsP_3$ pathways in neurons. Neuron *14*, 209–220.

Eder, C. (2005). Regulation of microglial behavior by ion channel activity. J. Neurosci. Res. *81*, 314–321.

Fanger, C.M., Rauer, H., Neben, A.L., Miller, M.J., Rauer, H., Wulff, H., Rosa, J.C., Ganellin, C.R., Chandy, K.G., and Cahalan, M.D. (2001). Calcium-activated potassium channels sustain calcium signaling in T lymphocytes. Selective blockers and manipulated channel expression levels. J. Biol. Chem. *276*, 12249–12256.

Frieden, M., Sollini, M., and Beny, J. (1999). Substance P and bradykinin activate different types of KCa currents to hyperpolarize cultured porcine coronary artery endothelial cells. J. Physiol. *519*, 361–371.

Gimpl, G., Walz, W., Ohlemeyer, C., and Kettenmann, H. (1992). Bradykinin receptors in cultured astrocytes from neonatal rat brain are linked to physiological responses. Neurosci. Lett. *144*, 139–142.

Hall, J.M. (1992). Bradykinin receptors: pharmacological properties and biological roles. Pharmacol. Ther. *56*, 131–190.

Hallberg, M. and Nyberg, F. (2003). Neuropeptide conversion to bioactive fragments – an important pathway in neuromodulation. Curr. Protein Pept. Sci. *4*, 31–44.

Hanani, M. (2005). Satellite glial cells in sensory ganglia: from form to function. Brain Res. Brain Res. Rev. *48*, 457–476.

He, M., Howe, D.G., and McCarthy, K.D. (1996). Oligodendroglial signal transduction systems are regulated by neuronal contact. J. Neurochem. *67*, 1491–1499.

Heitsch, H. (2000). Bradykinin B2 receptor as a potential therapeutic target. Drug News Perspect. *13*, 213–225.

Higashida, H. and Brown, D.A. (1988). Ca^{2+}-dependent K^+ channels in neuroblastoma hybrid cells activated by intracellular inositol trisphosphate and extracellular bradykinin. FEBS Lett. *238*, 395–400.

Honda, S., Sasaki, Y., Ohsawa, K., Imai, Y., Nakamura, Y., Inoue, K., and Kohsaka, S. (2001). Extracellular ATP or ADP induce chemotaxis of cultured microglia through $G_{i/o}$-coupled P2Y receptors. J. Neurosci. *21*, 1975–1982.

Hosli, L., Hosli, E., Kaeser, H., and Lefkovits, M. (1992). Colocalization of receptors for vasoactive peptides on astrocytes of cultured rat spinal cord and brain stem: electrophysiological effects of atrial and brain natriuretic peptide, neuropeptide Y and bradykinin. Neurosci. Lett. *148*, 114–116.

Ifuku, M., Wang, B., and Noda, M. (2005). Activation of Ca^{2+}-dependent K^+ channels is essential for bradykinin-induced microglial migration. In: VII European Meeting on Glial Cell Function in Health and Disease, 19–25 May 2005, Amsterdam, Netherlands (Bologna, Italy: Medimond S.r.l.), pp. 97–101.

Kaeser, F., Luthy, C., Herschkowitz, N., and Oetliker, O. (1988). The effect of temporary hypoxia on prostaglandin synthesis in mouse brain cell cultures during development. Prostaglandins Leukot. Essent. Fatty Acids *32*, 75–81.

Kim, E.J., Kwon, K.J., Park, J.Y., Lee, S.H., Moon, C.H., and Baik, E.J. (2002). Neuroprotective effects of prostaglandin E_2 or cAMP against microglial and neuronal free radical mediated toxicity associated with inflammation. J. Neurosci. Res. *70*, 97–107.

Kim, S.J. and Kim, J. (1998). Relation of exocytosis and Ca^{2+}-activated K^+ current during Ca^{2+} release from intracellular stores in individual rat chromaffin cells. Brain Res. *799*, 197–206.

Kim, S.U. and de Vellis, J. (2005). Microglia in health and disease. J. Neurosci. Res. *81*, 302–313.

Kreutzberg, G.W. (1996). Microglia: a sensor for pathological events in the CNS. Trends Neurosci. *19*, 312–318.

Lehnardt, S., Massillon, L., Follett, P., Jensen, F.E., Ratan, R., Rosenberg, P.A., Volpe, J.J., and Vartanian, T. (2003). Activation of innate immunity in the CNS triggers neurodegeneration through a Toll-like receptor 4-dependent pathway. Proc. Natl. Acad. Sci. USA *100*, 8514–8519.

Liebmann, C. (2001). Bradykinin signalling to MAP kinase: cell-specific connections versus principle mitogenic pathways. Biol. Chem. *382*, 49–55.

Liebmann, C., Offermanns, S., Spicher, K., Hinsch, K.D., Schnittler, M., Morgat, J.L., Reissmann, S., Schultz, G., and Rosenthal, W. (1990). A high-affinity bradykinin receptor in membranes from rat myometrium is coupled to pertussis toxin-sensitive G proteins of the G_i family. Biochem. Biophys. Res. Commun. *167*, 910–917.

Lin, W.W. and Chuang, D.M. (1992). Regulation of bradykinin-induced phosphoinositide turnover in cultured cerebellar astrocytes: possible role of protein kinase C. Neurochem. Int. *21*, 573–579.

Miura, H., Liu, Y., and Gutterman, D.D. (1999). Human coronary arteriolar dilation to bradykinin depends on membrane hyperpolarization: contribution of nitric oxide and Ca^{2+}-activated K^+ channels. Circulation *99*, 3132–3138.

Nimmerjahn, A., Kirchhoff, F., and Helmchen, F.R. (2005). Resting microglial cells are highly dynamic surveillants of brain parenchyma *in vivo*. Science *308*, 1314–1318.

Noda, M., Kariura, Y., Amano, T., Manago, Y., Nishikawa, K., Aoki, S., and Wada, K. (2003). Expression and function of bradykinin receptors in microglia. Life Sci. *72*, 1573–1581.

Noda, M., Kariura, Y., Amano, T., Manago, Y., Nishikawa, K., Aoki, S., and Wada, K. (2004a). Kinin receptors in cultured rat microglia. Neurochem. Int. *45*, 437–442.

Noda, M., Kariura, Y., Kosai, Y., Pannasch, U., Wang, L., Kettenmann, H., Nishikawa, K., Okada, S., Aoki, S., and Wada, K. (2004b). Inflammation in the CNS: the role of bradykinin in glial cells. J. Neurochem. *88* (Suppl. 1), 11.

Parpura, V., Basarsky, T.A., Liu, F., Jeftinija, K., Jeftinija, S., and Haydon, P.G. (1994). Glutamate-mediated astrocyte-neuron signalling. Nature *369*, 744–747.

Perry, V.H., Andersson, P.B., and Gordon, S. (1993). Macrophages and inflammation in the central nervous system. Trends Neurosci. *16*, 268–273.

Raidoo, D.M. and Bhoola, K.D. (1998). Pathophysiology of the kallikrein-kinin system in mammalian nervous tissue. Pharmacol. Ther. *79*, 105–127.

Ritchie, T., Cole, R., Kim, H.S., de Vellis, J., and Noble, E.P. (1987). Inositol phospholipid hydrolysis in cultured astrocytes and oligodendrocytes. Life Sci. *41*, 31–39.

Schilling, T., Stock, C., Schwab, A., and Eder, C. (2004). Functional importance of Ca^{2+}-activated K^+ channels for lysophosphatidic acid-induced microglial migration. Eur. J. Neurosci. *19*, 1469–1474.

Schwaninger, M., Sallmann, S., Petersen, N., Schneider, A., Prinz, S., Libermann, T.A., and Spranger, M. (1999). Bradykinin induces interleukin-6 expression in astrocytes through activation of nuclear factor-κB. J. Neurochem. *73*, 1461–1466.

Scicli, A.G., Forbes, G., Nolly, H., Dujovny, M., and Carretero, O.A. (1984). Kallikrein-kinins in the central nervous system. Clin. Exp. Hypertens. A *6*, 1731–1738.

Shie, F.S., Montine, K.S., Breyer, R.M., and Montine, T.J. (2005). Microglial EP2 as a new target to increase amyloid beta phagocytosis and decrease amyloid β-induced damage to neurons. Brain Pathol. *15*, 134–138.

Simpson, P.B., Mehotra, S., Lange, G.D., and Russell, J.T. (1997). High density distribution of endoplasmic reticulum proteins and mitochondria at specialized Ca^{2+} release sites in oligodendrocyte processes. J. Biol. Chem. *272*, 22654–22661.

Stephens, G.J., Marriott, D.R., Djamgoz, M.B., and Wilkin, G.P. (1993a). Electrophysiological and biochemical evidence for bradykinin receptors on cultured rat cortical oligodendrocytes. Neurosci. Lett. *153*, 223–226.

Stephens, G.J., Cholewinski, A.J., Wilkin, G.P., and Djamgoz, M.B. (1993b). Calcium-mobilizing and electrophysiological effects of bradykinin on cortical astrocyte subtypes in culture. Glia *9*, 269–279.

Su, Y., Ganea, D., Peng, X., and Jonakait, G.M. (2003). Galanin down-regulates microglial tumor necrosis factor-α production by a post-transcriptional mechanism. J. Neuroimmunol. *134*, 52–60.

Tzeng, S.F., Hsiao, H.Y., and Mak, O.T. (2005). Prostaglandins and cyclooxygenases in glial cells during brain inflammation. Curr. Drug Targets Inflamm. Allergy *4*, 335–340.

Ubink, R., Calza, L., and Hokfelt, T. (2003). 'Neuro'-peptides in glia: focus on NPY and galanin. Trends Neurosci. *26*, 604–609.

Walker, K., Perkins, M., and Dray, A. (1995). Kinins and kinin receptors in the nervous system. Neurochem. Int. *26*, 1–16.

Wang, H., Kohno, T., Amaya, F., Brenner, G.J., Ito, N., Allchorne, A., Ji, R.R., and Woolf, C.J. (2005). Bradykinin produces pain hypersensitivity by potentiating spinal cord glutamatergic synaptic transmission. J. Neurosci. *25*, 7986–7992.

Webb, J.G., Shearer, T.W., Yates, P.W., Mukhin, Y.V., and Crosson, C.E. (2003). Bradykinin enhancement of PGE_2 signalling in bovine trabecular meshwork cells. Exp. Eye. Res. *76*, 283–289.

Welsh, C., Dubyak, G., and Douglas, J.G. (1988). Relationship

between phospholipase C activation and prostaglandin E_2 and cyclic adenosine monophosphate production in rabbit tubular epithelial cells. Effects of angiotensin, bradykinin, and arginine vasopressin. J. Clin. Invest. *81*, 710–719.

Yanaga, F., Hirata, M., and Koga, T. (1991). Evidence for coupling of bradykinin receptors to a guanine-nucleotide binding protein to stimulate arachidonate liberation in the osteoblast-like cell line, MC3T3-E1. Biochim. Biophys. Acta *1094*, 139–146.

Available online at www.sciencedirect.com
SCIENCE DIRECT®
Biochemical and Biophysical Research Communications 342 (2006) 867–874
BBRC
www.elsevier.com/locate/ybbrc

TrkB-T1 regulates the RhoA signaling and actin cytoskeleton in glioma cells

Koji Ohira [a,b], Koichi J. Homma [c], Hirohisa Hirai [a], Shun Nakamura [b], Motoharu Hayashi [a,*]

[a] *Department of Cellular and Molecular Biology, Primate Research Institute, Kyoto University, Aichi, Japan*
[b] *Department of Biochemistry and Cellular Biology, National Institute of Neuroscience, National Center of Neurology and Psychiatry, Tokyo, Japan*
[c] *Department of Molecular Pathology, Faculty of Pharmaceutical Sciences, Teikyo University, Kanagawa, Japan*

Received 30 January 2006
Available online 20 February 2006

Abstract

Recently, the truncated TrkB receptor, T1, has been reported to be involved in the control of cell morphology via the regulation of Rho proteins, through which T1 binds Rho guanine nucleotide dissociation inhibitor (Rho GDI) 1 and dissociates it in a brain-derived neurotrophic factor (BDNF)-dependent manner. However, it is unclear whether T1 signaling regulates the downstream of Rho signaling and the actin cytoskeleton. In this study, we investigated this question using C6 rat glioma cells, which express T1 endogenously. Rho GDI1 was dissociated from T1 in a BDNF-dependent manner, which also causes decreases in the activities of Rho-signaling molecules such as RhoA, Rho-associated kinase, p21-activated kinase, and extracellular-signal regulated kinase1/2. Moreover, BDNF treatment resulted in the disappearance of stress fibers in the cells treated with lysophosphatidic acid, an activator of RhoA, and in morphological changes in cells. Furthermore, a competitive assay with cyan fluorescent protein fusion proteins of T1-specific sequences reduced the effects of BDNF. These results suggest that T1 regulates the Rho-signaling pathways and the actin cytoskeleton.

Keywords: BDNF; Cell morphology; ERK; In vitro; Neurotrophin; PAK; ROCK; Signal transduction; TrkB receptor

Neurotrophins belong to the nerve growth factor (NGF) family and in mammals consist of NGF, brain-derived neurotrophic factor (BDNF), NT-3, and NT-4. Their receptors are the tropomyosin related kinase (Trk) receptor family. TrkA recognizes NGF, both BDNF and NT-4 are ligands for TrkB, and TrkC is an NT-3 receptor [1].

In the mammalian central nervous system (CNS), BDNF, and TrkB are enriched [2–4] and function as survival, differentiation, morphogenic, and growth factors during early development, and as mediators of neural plasticity in the adult stage [5,6]. The TrkB gene encodes at least three subtypes: TK+, T1, and T2 [1]. TK+ has its signaling pathways via tyrosine kinases such as Ras, phosphatidylinositide 3-kinase, and phospholipase C-γ [7]. In contrast, T1 and T2 possess specific 11- and 9-amino acid sequences, respectively, in the C-terminal instead of tyrosine kinases. The T1-specific amino acid sequence is completely conserved from mice to humans [8–10]. Furthermore, the TrkB subtypes show characteristic expression patterns during the development of the mammalian CNS [4,11,12]. TK+ is detected at the same levels from embryonic to adult periods, while the expression of T1 increases remarkably during the late developmental period and is maintained to adulthood. Moreover, in the prefrontal cortex of the adult monkey, TK+ homodimer cannot be detected, but T1 homodimer and TK+–T1 heterodimer are formed in a BDNF-dependent manner [13]. Thus, these findings suggest that T1 plays an important role in such functions as neural plasticity and maintenance during the adult period.

Recently, T1 has been reported to regulate the morphology of both neurons [14,15] and glias [16,17] as well as calcium entry into astrocytes [18]. For example, the

* Corresponding author. Fax: +81 568 63 0085.
E-mail address: hayashi@pri.kyoto-u.ac.jp (M. Hayashi).

0006-291X/$ - see front matter © 2006 Elsevier Inc. All rights reserved.
doi:10.1016/j.bbrc.2006.02.033

overexpression of T1 induces the elongation of and an increase in the branch number of distal dendrites of cortical pyramidal neurons in slices [14]. In hippocampal cultures, T1 expression has been found to increase the number of dendritic filopodia [15]. Both reports point out that the T1-induced elongation of dendrites and filopodia occurs independently of ligand binding. Therefore, it is of great interest to elucidate the T1 signaling mechanism; nevertheless, this mechanism remains unclear to date, a decade after the discovery of T1. Most recently, T1 has been reported to regulate cell morphology via Rho guanine nucleotide dissociation inhibitor (Rho GDI) 1 in primary astrocytic cultures [16]. Rho GDI1 is a negative regulator of Rho GTPases [19], which may explain in part the previous data that T1 regulates neuronal morphology [14,15]. However, it remains unclear whether T1 regulates the downstream effectors of its signaling pathway and the actin cytoskeleton. In the present study, we elucidate the missing link between Rho GDI1 and cell morphology.

Materials and methods

Cell culture. C6 cells (Dainippon Pharmaceutical, Osaka, Japan) were maintained in Ham's F-10 (Gibco, Rockville, MD, USA) supplemented with 15% horse serum (Gibco) and 2.5% fetal bovine serum (Gibco) in a humidified atmosphere containing 5% CO_2 at 37 °C. In this experiment, cells were cultured to subconfluency (70–80%) in 10-cm dishes in serum-free Ham's F-10 containing N2 supplement (Gibco) for 24 h. For administration of reagents, cells were stimulated for 30 min at 37 °C with 20 ng/ml BDNF (PeproTech, Rocky Hill, NJ, USA), anti-BDNF antibody (5 μg/ml, Santa Cruz Biotechnology, Santa Cruz, CA, USA), anti-p75 antibody (clone MC192, 1/50 of culture medium), or 10 μM LPA (Sigma, St. Louis, MO, USA). Cells were also incubated with one reagent for 30 min and subsequently incubated with another for 30 min.

Reverse transcription-polymerase chain reaction (RT-PCR). Total RNA was isolated from the cortex of adult Wistar rats (2 males, 3 months old) or C6 cells using ISOGEN (Nippon Gene, Tokyo, Japan). Reverse transcription was performed with superscript-II (Gibco) and the cDNA was amplified by PCR with primers specific for TK+ (603 bp), 5′-TCAGCAACGACGATGACTCT-3′ and 5′-AGTGTTGGGATGC CAGGTAG-3′; T1 (615 bp), 5′-CCTCGTCGGAGAAGATCAAG-3′ and 5′-TCCAGGGGGATCTTATGAAA-3′; T2 (598 bp), 5′-CAGA AAACCTCGTCGGAGAA-3′ and 5′-TGCTTACCTTTCATGCCAAA-3′; and actin (349 bp), 5′-TAAAACGCAGCTCAGTAACAGTCCG-3′ and 5′-TGGAATCCTGTGGCATCCATGAAAC-3′. The PCR was carried out as follows: DNA was denatured for 2 min at 94 °C and sequences were amplified for 30 cycles (94 °C for 30 s; 58 °C for 30 s; 72 °C for 60 s). The PCR products were separated on 2% agarose gel.

DNA constructs and transfection. We used the DNA constructs created in our previous study [16]. Briefly, vectors of enhanced cyan fluorescent protein (ECFP)-Δ11 and ECFP-ICD were prepared by PCR, using the 5′ primer, GGTCTGCCGTCTGCACGTCTG, and the 3′ primers Δ11, CGCGGATCCTTAACCTTTCATGCC; and ICD, CGCGGATCC CCCAGCCTTGTCTTTCCTTTATC. Underlining indicates *Bam*HI sites, and boldface letters represent mutation sites. The PCR products were first digested by *Bam*HI and were then subcloned into pECFP-C1 (Clontech, Palo Alto, CA, USA). These constructs were transfected into C6 cells (50% confluent) with FuGENE6 (Roche, Basel, Switzerland).

Precipitation assays. Cells plated in a 10-cm dish were lysed with 200 μl of lysis buffer (for co-immunoprecipitation of TrkB, 10 mM triethanolamine, 10 mM iodoacetamine, pH 7.8, 150 mM NaCl, 2 mM EDTA, 1% digitonin, 1 mM phenylmethylsulfonyl fluoride (PMSF), 10 μg/ml leupeptin, and 20 μg/ml aprotinin; for precipitation of RhoA, phosphorylated PAK, phosphorylated Rho-associated kinase (ROCK), 50 mM Tris–HCl, pH 7.5, 150 mM NaCl, 5 mM MgCl2, 0.5% Triton X-100, 1 mM PMSF, 10 μg/ml leupeptin, 20 μg/ml aprotinin, and 10 nM microcystin LR). The lysates were centrifuged at 10,000*g* at 4 °C for 20 min, and the protein contents of the supernatants were determined and adjusted at 1 mg total protein/ml.

For the precipitation of TrkB, PAK, and ROCK, after incubation with preimmune IgG-protein A or G (Amersham Pharmacia Biotechnology, Tokyo, Japan) at 4 °C for 1 h, the supernatants were incubated with the indicated antibodies at 4 °C for 1 h and then with 20 μl of protein A or G Sepharose at 4 °C for 1 h. The complexes were washed once with lysis buffer containing 300 mM NaCl and 3× with lysis buffer. They were then mixed with 40 μl sodium dodecyl sulfate (SDS) sample buffer and boiled for 3 min.

For the RhoA pull-down assay, we used Rhotekin beads (Upstate Biotechnology, Charlottesville, VA, USA) following the method described by Ren et al. [20]. Briefly, the Rhotekin beads (30 μl) were added to the lysates (500 μg protein/ml) and incubated at 4 °C for 45 min. The beads were then washed 3× with lysis buffer. The resultant pellets were mixed with 40 μl SDS sample buffer and boiled for 3 min.

Western blot analysis. Samples (5 μg/lane for Rho GDI1, RhoA, ERK1/2, PAK, and ROCK; 150 μg/lane for TrkB; 20 μl for precipitation) were subjected to SDS–polyacrylamide gel electrophoresis (PAGE) (7% gel for TrkB and ROCK, 10% gel for extracellular-signal regulated kinase (ERK) 1/2 and PAK, and 12% gel for Rho GDI1 and RhoA) and blotted onto polyvinylidene difluoride (PVDF) membranes (Millipore, Billerica, MA, USA). The membranes were blocked in 5% skim milk in phosphate-buffered saline (PBS). After incubation with the indicated antibodies at room temperature for 1 h, blots were incubated with the secondary antibodies conjugated with horseradish peroxidase (HRP) and visualized by the enhanced chemiluminescence (ECL) system (Amersham Pharmacia Biotechnology).

Immunocytochemistry. Cells were grown on 12-mm diameter plastic sheets at 1000 cells/30 mm dish. The cells were fixed for 20 min in 3.7% formaldehyde in PBS and permeabilized for 20 min in PBS containing 0.1% Triton X-100. To retrieve the antigenicity of T1, the samples were preincubated in 6 M guanidine chloride in 50 mM Tris–HCl, pH 10.2, at room temperature for 15 min [16,17,21,22]. The samples were incubated at room temperature for 1 h with anti-TK+ antibody (diluted at 1/1600; Santa Cruz Biotechnology), anti-T1 antibody (diluted at 1/1600; Santa Cruz Biotechnology), or vehicle as control (PBS containing 4% normal goat serum and 1% bovine serum albumin (BSA)). They were incubated with a biotinylated secondary antibody at room temperature for 1 h. The immunoreactive sites were visualized by the avidin–biotin complex peroxidase method using an ABC elite kit (Vector Laboratories, Burlingame, CA, USA). A solution of 0.3% H_2O_2, 20 μg/ml 3,3′-diaminobenzidine tetrahydrochloride, and 0.3% nickel ammonium sulfate in 0.05 M Tris–HCl buffer, pH 7.6, was used as the substrate of the peroxidase. The plastic sheets were mounted on glass slides with Permafluor (Thermo Shandon, Pittsburgh, PA, USA).

Morphology assay. Fixed cells were incubated with 0.1 μg/ml fluorescein isothiocyanate (FITC)-phalloidin (Molecular Probes, Eugene, OR, USA) at room temperature for 20 min. The cells were counterstained with propidium iodide to visualize nuclei [23]. The samples were analyzed using a phase contrast microscope and a Zeiss confocal microscope (LSM 510; Carl Zeiss Japan, Tokyo, Japan). Three different morphologies were distinguished: (1) fully round, or round shape with extensions shorter than the soma diameter; (2) spindle or round shape with extensions longer than the soma diameter; (3) flat shape with thinly stretched extensions.

Results

Expression of T1 in C6 cells

Neurons have been found to contain both TK+ and T1 [16,17,21,22,24], while glial cells express primarily T1 [16,24]. Thus, we made use of C6 cells derived from rat

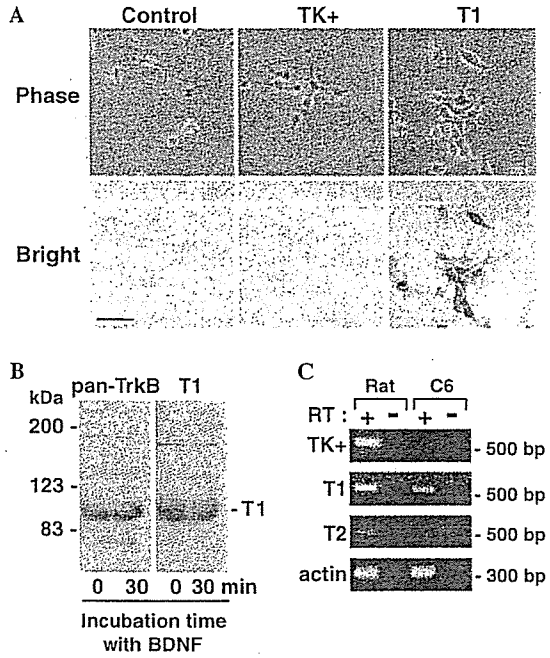

Fig. 1. Expression of the truncated TrkB receptor, T1, in C6 cells. (A) Immunocytochemistry of TK+ and T1 in C6 cells. Scale bar, 30 μm. (B) Western blot analysis of T1 in C6 cells, using anti-pan-TrkB and anti-T1 antibodies, at 0 and 30 min after stimulation with BDNF (20 ng/ml). (C) RT-PCR analysis of TrkB expression in the cerebral cortex of adult rats (3 months old) and C6 cells. BDNF, brain-derived neurotrophic factor; RT, reverse transcription.

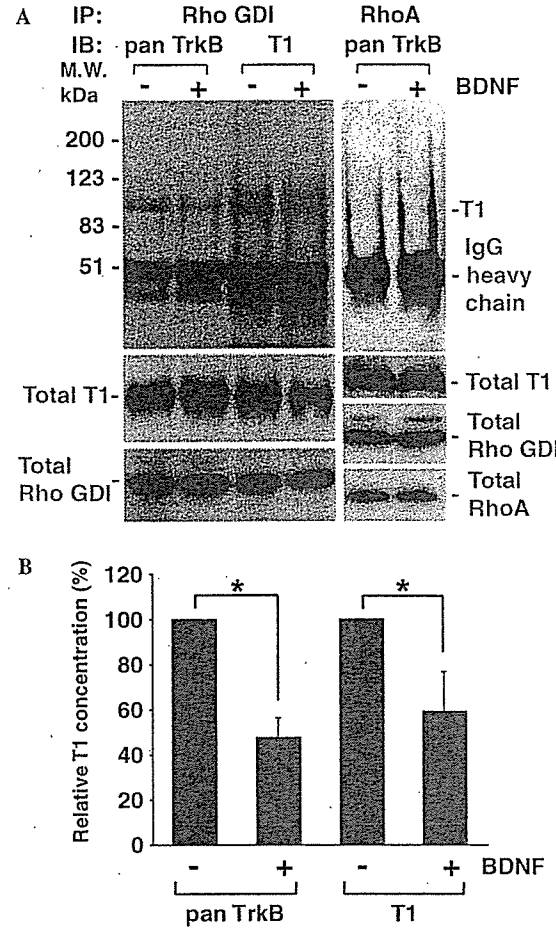

Fig. 2. Dissociation of Rho GDI1 from T1 by BDNF. (A) Co-immunoprecipitation of T1 with anti-Rho GDI1 (left column) or anti-RhoA (right column) after BDNF stimulation (20 ng/ml). T1 was detected with anti-pan-TrkB or T1 antibody. IP, immunoprecipitation; IB, immunoblot; M.W., molecular weight. (B) Quantitative analysis of the bands in (A). Control levels were taken as 100%. The asterisks indicate statistically significant differences ($p < 0.05$ by paired Student's t test). Values are given as means ± SD from four independent experiments.

glioma cells to investigate the signaling mechanism of T1; detected T1, but not TK+, in these cells (Fig. 1). We further confirmed by RT-PCR analysis that only T1 mRNA is expressed in C6 cells (Fig. 1C), and that the BDNF treatment did not induce TK+ within 30 min (Fig. 1B). Furthermore, we did not detect any expression of Rac or Cdc42 at the protein level by Western blot analysis (data not shown), which is consistent with previous results [25]. Thus, we focused primarily on analyzing the RhoA-signaling mechanism in C6 cells.

BDNF-induced dissociation of Rho GDI1 from T1

Using C6 cells, we examined whether BDNF stimulation dissociated Rho GDI1 from T1 in a BDNF-dependent manner. After BDNF stimulation (final concentration, 20 ng/ml), the T1 band was reduced to ≈50% of the control value (Fig. 2), suggesting that treatment with BDNF causes Rho GDI1 to dissociate from T1; this result is consistent with our previous results [16]. In addition, RhoA was not directly bound to T1 (right column in Fig. 2A).

Control of Rho-signaling pathways

Rho GDI1 has been shown to interact with guanosine diphosphate (GDP)-bound forms of Rho guanosine triphosphatases (GTPases) and to inhibit their conversion from GDP-bound inactive forms to guanosine triphosphate (GTP)-bound active forms [19]. Next, we investigated the effect of T1-Rho GDI1 on RhoA activated by LPA and performed a pull-down assay of the active form of RhoA. LPA treatment (10 μM) was found to increase the activity of RhoA up to 170% of the control value (Fig. 3A). Moreover, the RhoA activation triggered by LPA was reduced to the control level by BDNF treatment (20 ng/ml).

Among the numerous effector molecules of RhoA, ROCK is interesting since it is involved in various cellular functions, such as the control of smooth muscle contraction and stress fiber formation. This effect is mediated by the phosphorylation of the myosin light chain and LIM (LIM is an acronym of the three gene products Lin-11, Isl-1, and Mec-3) kinase, and the inactivation of myosin phosphatase [19,26,27]. Next, we examined whether ROCK is involved in T1 signaling. ROCK phosphorylation was found to increase significantly to 138% of the control level

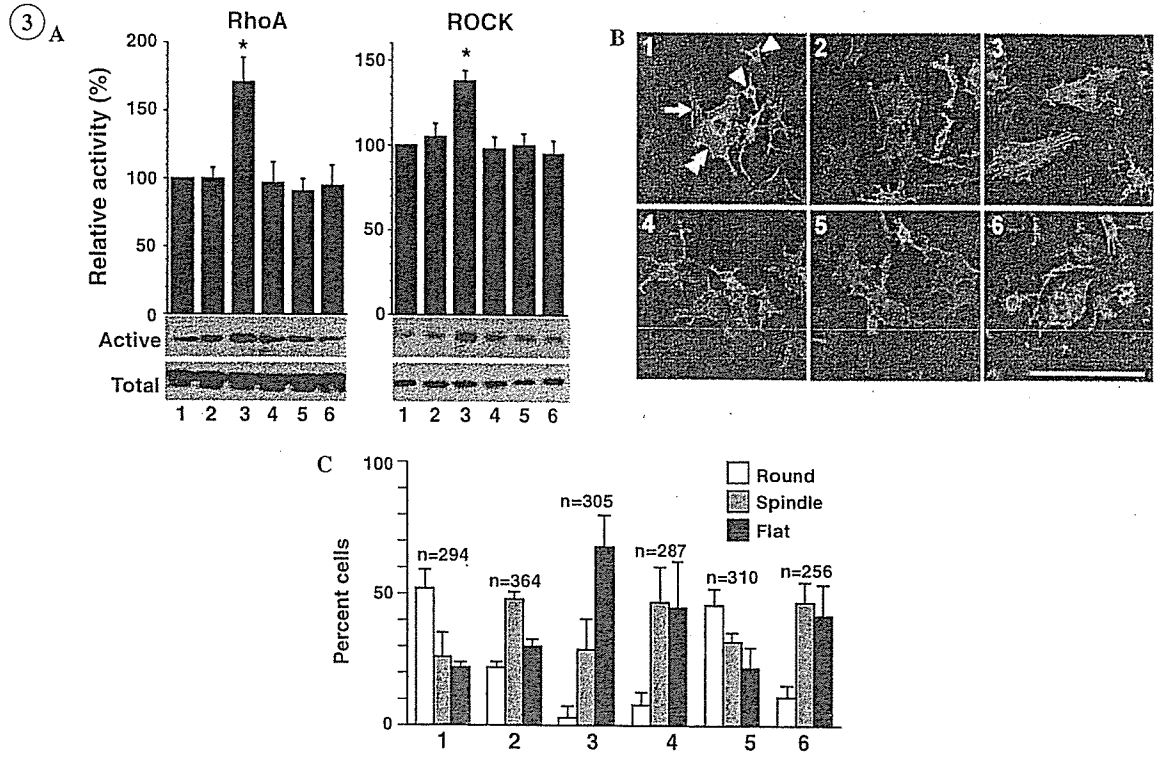
3
A
RhoA
ROCK
Relative activity (%)
Active
Total
1 2 3 4 5 6
B
C
Percent cells
Round
Spindle
Flat
n=294
n=364
n=305
n=287
n=310
n=256

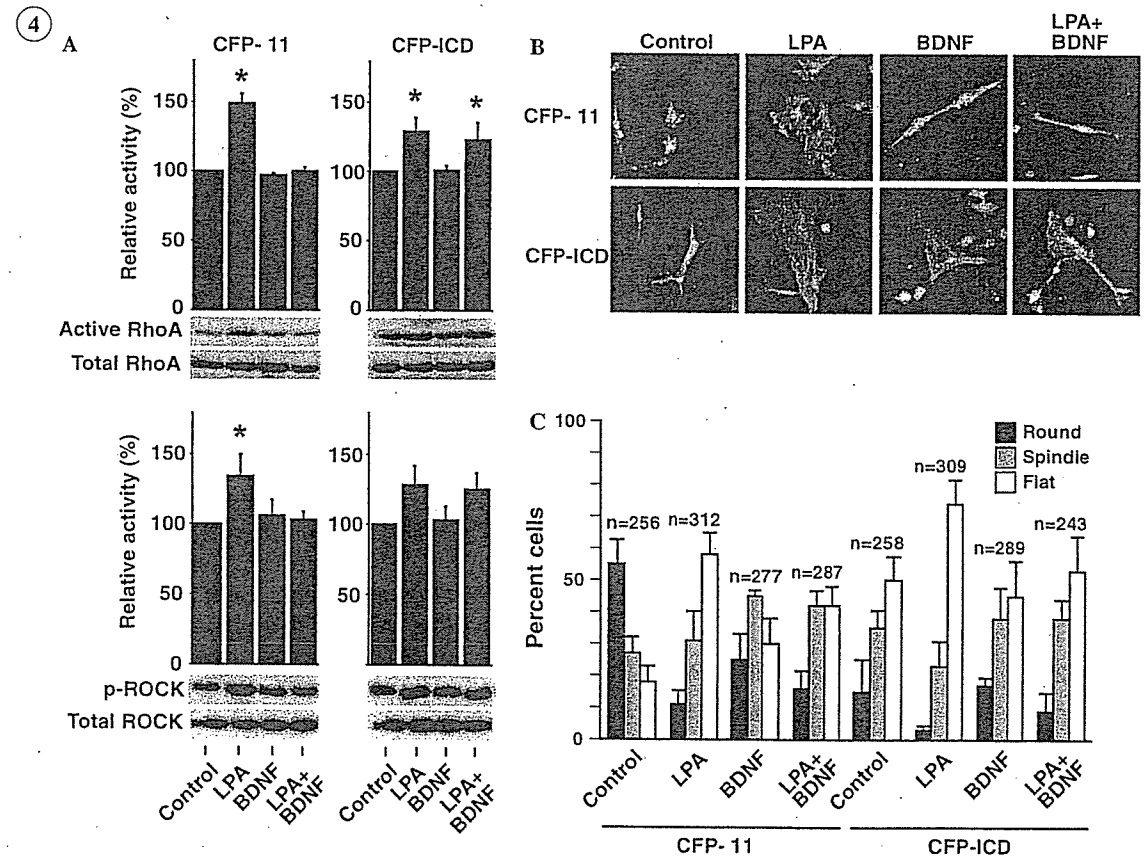
4
A
CFP- 11
CFP-ICD
Relative activity (%)
Active RhoA
Total RhoA
p-ROCK
Total ROCK
Control
LPA
BDNF
LPA+ BDNF
B
Control
LPA
BDNF
LPA+ BDNF
CFP- 11
CFP-ICD
C
Percent cells
Round
Spindle
Flat
n=256
n=312
n=277
n=287
n=258
n=309
n=289
n=243
CFP- 11
CFP-ICD

by LPA treatment (10 μM) (Fig. 3A), while BDNF alone did not alter the phosphorylation of ROCK. On the other hand, the LPA-induced phosphorylation of ROCK was reduced to the control level by BDNF stimulation. Thus, ROCK activity was found to correlate with RhoA activity in the present study.

Recently, it has been reported that p75 associates with Rho GDI1 and regulates Rho activity [28]. In order to examine the contribution of p75 in the present experiment, cells were incubated during operations with an anti-p75 antibody, clone MC192, which inhibits the interaction between p75 and Trk receptors [15,29]. If there were a contribution of p75 in the present experiment, the activities of RhoA and ROCK would be maintained at a high level in the cells treated by LPA + BDNF, that is, when BDNF action is inhibited. However, we found that the anti-p75 antibody treatment had no effect on BDNF action, which reduced the high activity levels of RhoA and ROCK induced by LPA (Fig. 3A, lane 6). Therefore, it is unlikely that p75 contributed to the regulation of Rho proteins in our experiment.

Changes in C6 cell morphology due to T1-Rho GDI1

It is known that Rho proteins can regulate cell morphology via remodeling of the actin cytoskeleton [30]. Thus, we examined the effect of BDNF on cell morphology and on the reorganization of the actin cytoskeleton. C6 cells tended to show a rounded shape and modest stress fiber staining in the cell periphery in the control samples (Figs. 3B and C). In contrast, LPA (10 μM)-treated cells showed a flattened shape (68%) and strong stress fiber bundles. When cells were treated with BDNF (20 ng/ml), the percentage of spindle-shaped cells (48%) was greater than that of the control (26%) and that of LPA-treated (29%) cells. We next examined whether the LPA-induced production of stress fibers could be blocked by BDNF stimulation. The cells were first treated with LPA for 30 min and then incubated with BDNF for 30 min. Subsequent staining of the cells showed fewer or no stress fibers. In addition, the percentage of spindle-shaped cells increased from 29% to 48%, while that of flat-shaped cells decreased from 68% to 45% compared with the LPA-treated cells. Furthermore, anti-BDNF antibody was able to inhibit the BDNF action, suggesting that this effect is BDNF-specific. On the other hand, anti-p75 antibody did not inhibit the effect of BDNF on cell morphology and actin remodeling, suggesting that p75 is not involved in the regulation of cell morphology or actin remodeling.

Competitive assay with T1 intracellular peptides

To further examine the inhibitory effect of the intracellular domain of T1 for Rho signaling, we carried out the transfection of the pCFP-intracellular domain of T1, CFP-Δ11, and CFP-ICD, in order to inhibit the T1 signaling cascade in a competitive manner. We expected that CFP-ICD, but not CFP or CFP-Δ11, would trap Rho GDI1 within the cytoplasmic region and inhibit the association of Rho GDI1 with the Rho GTPases, thereby resulting in the inhibition of the BDNF effect. When CFP (data not shown) and CFP-Δ11 were expressed, the changes in cell morphology were comparable with those of untransfected cells (Figs. 3 and 4), suggesting that the first 12 intracellular amino acids of T1 are not affected by changes in C6 cell morphology. In contrast, the cells expressing CFP-ICD showed spindle or flat shapes even under no treatment conditions. Moreover, the CFP-ICD was able to reduce the BDNF effect which transforms a flat cell into a spindle-shaped cell, suggesting that the T1-specific sequence is important in BDNF-dependent C6 morphological regulation.

Control of the PAK-signaling cascade by T1

Recently, Rho family proteins have been reported to upregulate the PAK activity that is involved in the regulation of axon growth [31], which can activate both Raf and mitogen-activated protein kinase (MEK), leading to ERK activation [32–34]. Thus, to confirm that T1-Rho GDI1 signaling could regulate the other effectors of Rho proteins, we examined whether T1 regulates the phosphorylation of PAK and ERK. Phosphorylated PAK was significantly

Fig. 3. Regulation of the Rho-signaling cascade and morphological changes in C6 cells. 1, control; 2, BDNF (10 ng/ml); 3, LPA (10 μM); 4, LPA + BDNF; 5, anti-BDNF (5 μg/ml) + BDNF; 6, MC192 (1/50 of culture medium) + LPA + BDNF. (A) Analysis of RhoA and ROCK activities in C6 cells. Control levels were taken as 100%. The asterisks indicate significant differences ($p < 0.05$ by one-way analysis of variance (ANOVA) and Scheffé's post hoc test) compared to control levels. Values are given as means ± SD and are the result of four independent experiments. (B) Confocal microscopic images. Green (FITC-phalloidin) and red (propidium iodide) represent actin fibers and cell nuclei, respectively. All panels are merged images. In Image 1, three types of cell morphology are seen: arrowhead, round type; double-arrowhead spindle type; arrow, flat type. Scale bar, 30 μm. (C) Populations of the three categories of cell morphology. Values are given as means ± SD of four independent experiments. The numbers indicate the total cell counts.

Fig. 4. Competitive assay using the fusion proteins of CFP and specific peptides of T1. (A) Analysis of RhoA and ROCK activities in C6 cells with CFP-Δ11 and CFP-ICD having been transfected. Control levels were taken as 100%. The asterisks indicate significant differences ($p < 0.05$ by one-way ANOVA and Scheffé's post hoc test) from the levels of the controls. Values are given as means ± SD and are the result of four independent experiments. (B) Confocal microscopic images of changes in the morphology and stress fibers of C6 cells. Green (FITC-phalloidin), red (propidium iodide), and blue (CFP) represent actin fibers, cell bodies, and overexpressing CFP-fusion proteins, respectively. All panels are merged images. Scale bar, 30 μm. (C) Populations of the three categories of cell morphology. Values are given as means ± SD and are the result of four independent experiments. The numbers indicate the total cell counts.

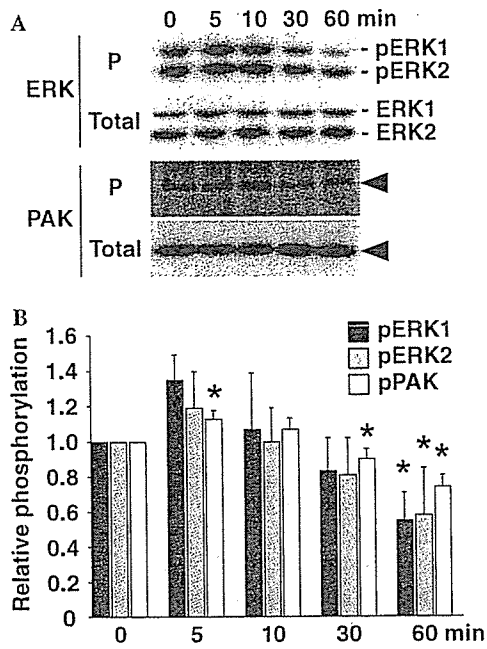

Fig. 5. Phosphorylation of PAK and ERK1/2 in C6 cells. (A) Western blot analysis of PAK and ERK1/2 phosphorylation. P indicates phosphorylated proteins. (B) Quantitative analysis of the bands in (A). The asterisks indicate values that were significantly different ($p < 0.05$ by one-way ANOVA and Scheffé's post hoc test) from control values. The results of four experiments are shown as means ± SD. The horizontal axis shows the progress time after BDNF administration, and the vertical axis shows the percentage of phosphorylation. The levels at 0 min were taken as 100%.

increased up to 113% by BDNF stimulation at 5 min and significantly decreased to 88% and 75% of the control levels at 30 and 60 min, respectively (Fig. 5). Following an increase of phosphorylated ERK1/2 after BDNF stimulation, the phosphorylated ERK1/2, albeit not significantly, decreased to below control levels within 30 min (ERK1, 80%; ERK2, 77%) and was significantly reduced to approximately 60% of control levels at 60 min (ERK1, 57%; ERK2, 60%). Together, the activities of PAK and ERK were well correlated with those of RhoA and ROCK, suggesting that T1-Rho GDI1 signaling may regulate PAK and ERK activities.

Discussion

In the present study, we demonstrated that a truncated TrkB receptor, T1, is capable of ligand-mediated signaling through the T1- Rho GDI1 pathway, which acts negatively for Rho and ERK-signaling cascades in a BDNF-dependent manner, and that T1-Rho GDI1 signaling regulates the cellular morphology of glioma cells via remodeling of the actin cytoskeleton.

Control of Rho signaling and cell morphology by T1

The present results provide evidence that T1 signaling can negatively regulate the Rho and PAK-signaling pathways in a ligand-dependent manner. The substrates of Rho GDI1 are RhoA and -B, Rac1 and −2, and Cdc42. ROCK, a target protein of Rho, is involved in the formation of stress fiber and axon growth [35]. On the other hand, PAK plays an important role in actin remodeling for membrane ruffles and lamellipodium, and in the axon growth of neurons [31,36,37]. Thus, T1 signaling may cease the reorganization of the actin cytoskeleton. In addition, Rho proteins have been reported to regulate microtubules and intermediate filaments [30], suggesting that cell morphology may be determined by other such cytoskeleton elements.

The importance of the control of Rho proteins and the cytoskeleton by T1-Rho GDI1 signaling is hinted in a recent study by Horch et al. [38]. In their paper, they demonstrate that BDNF stimulation induces structural instability in dendrites and spines of neurons in the ferret visual cortex on postnatal days 25–28 [38], when T1 has already expressed in the ferret cerebral cortex [11]. Thus, the instability of dendrites and spines that might be induced by T1 may be attributed in part to preparation for the next morphological changes in cells.

The relationship between Rho proteins and cell morphology is more complicated than we tend to assume. For example, in mammalian neuroblastoma cells, Rho inhibits neurite outgrowth, while both Rac and Cdc42 promote neurite outgrowth [39,40]. However, in chick dorsal root ganglion neurons, the opposite occurs [41]. Therefore, the subcellular localization of Rho family proteins and T1 and/or the compositional rate of Rho proteins and their targets may determine how remodeling of the cytoskeleton occurs and thus how cells alter their shapes.

Control of ERK and PAK by T1

In the present study, we observed the upregulation of PAK and ERK1/2 phosphorylation within 5 min. This result was different from our expectations. One possible mechanism by which the phosphorylation of PAK and ERK is activated may involve the participation of low contents of TK+, which activates ERK1/2 via Ras-Raf-MEK1. The phosphorylation of ERK1/2 has been reported to be a very rapid reaction that occurs within 5 min [42]. There are two pathways by which ERK1/2 is activated, namely, the Ras- and Rho-dependent pathways, which converge on the Raf and MEK levels [32,34]. Therefore, after the activation of ERK by Rho signaling is stopped by Rho GDI1, the dephosphorylation of ERK1/2 by the endogenous phosphatases might be faster than the phosphorylation of ERK1/2 by Ras signaling. Consequently, the phosphorylation levels of ERK1/2 may decrease.

ERK1/2 is generally implicated in the regulation of growth responses of cells. It is of note that T1 has an inhibitory effect on ERK activation in C6 cells, while

TK+ can activate ERK1/2 via Ras. Therefore, T1 might cooperate with TK+ to confine BDNF functions spatiotemporally.

Acknowledgments

The authors thank Dr. Hans Thoenen for his helpful suggestions and comments. This work was supported by grants from the Ministry of Education, Culture, Sports, Science and Technology of Japan [No. 15016056 to M.H., No. 16015341 to S.N., Biodiversity Research of 21st Century COE (A14)], and the Organization of Pharmaceutical Safety and Research (Nano-1).

References

[1] M. Barbacid, The Trk family of neurotrophin receptors, J. Neurobiol. 25 (1994) 1386–1403.
[2] Q. Yan, M.J. Radeke, C.R. Matheson, J. Talvenheimo, A.A. Welcher, S.C. Feinstein, Immunocytochemical localization of TrkB in the central nervous system of the adult rat, J. Comp. Neurol. 378 (1997) 135–157.
[3] Q. Yan, R.D. Rosenfeld, C.R. Matheson, N. Hawkins, O.T. Lopez, L. Bennet, A.A. Welcher, Expression of brain-derived neurotrophic factor protein in the adult rat central nervous system, Neuroscience 78 (1997) 431–448.
[4] K. Ohira, K. Shimizu, M. Hayashi, Change of expression of full-length and truncated TrkBs in the developing monkey central nervous system, Dev. Brain Res. 112 (1999) 21–29.
[5] M. Bibel, Y.A. Barde, Neurotrophins: key regulators of cell fate and cell shapes in the vertebrate nervous system, Genes Dev. 14 (2000) 2919–2937.
[6] H. Thoenen, Neurotrophins and activity-dependent plasticity, Prog. Brain Res. 128 (2000) 183–191.
[7] R.A. Segal, Selectivity in neurotrophin signaling: theme and variations, Annu. Rev. Neurosci. 26 (2003) 299–330.
[8] R. Klein, D. Conway, L.F. Parada, M. Barbacid, The trkB tyrosine kinase gene codes for a second neurogenic receptor that lacks the catalytic kinase domain, Cell 61 (1990) 647–656.
[9] D.S. Middlemas, R.A. Lindberg, T. Hunter, TrkB, a neural receptor protein–tyrosine kinase: evidence for a full-length and two truncated receptors, Mol. Cell. Biol. 11 (1991) 143–153.
[10] D.L. Shelton, J. Sutherland, J. Gripp, T. Camerato, M.P. Armanini, H.S. Phillips, K. Carroll, S.D. Spencer, A.D. Levinson, Human trks: molecular cloning, tissue distribution, and expression of extracellular domain immunoadhesins, J. Neurosci. 15 (1995) 477–491.
[11] K.L. Allendoerfer, R.J. Cabelli, E. Escandon, D.R. Kaplan, K. Nikolics, C.J. Shatz, Regulation of neurotrophin receptors during the maturation of the mammalian visual system, J. Neurosci. 14 (1994) 1795–1811.
[12] R.H. Fryer, D.R. Kaplan, S.C. Feinstein, M.J. Radeke, D.R. Grayson, L.F. Kromer, Developmental and mature expression of full-length and truncated TrkB receptors in the rat forebrain, J. Comp. Neurol. 374 (1996) 21–40.
[13] K. Ohira, K. Shimizu, M. Hayashi, TrkB dimerization during development of the prefrontal cortex of the macaque, J. Neurosci. Res. 65 (2001) 463–469.
[14] T.A. Yacoubian, D.C. Lo, Truncated and full-length TrkB receptors regulate distinct modes of dendritic growth, Nat. Neurosci. 3 (2000) 342–349.
[15] M. Hartmann, T. Brigadski, K.S. Erdmann, B. Holtmann, M. Sendtner, F. Narz, V. Leßmann, Truncated TrkB receptor-induced outgrowth of dendritic filopodia involves the p75 neurotrophin receptor, J. Cell Sci. 117 (2004) 5803–5814.
[16] K. Ohira, H. Kumanogoh, Y. Sahara, K.J. Homma, H. Hirai, S. Nakamura, M. Hayashi, A truncated TrkB receptor, T1, regulates glial cell morphology via Rho GDP dissociation inhibitor 1, J. Neurosci. 25 (2005) 1343–1353.
[17] K. Ohira, K. Shimizu, A. Yamashita, M. Hayashi, Differential expression of the truncated TrkB receptor, T1, in the primary motor and prefrontal cortices of the adult macaque monkey, Neurosci. Lett. 385 (2005) 105–109.
[18] C.R. Rose, R. Blum, B. Pichler, A. Lepier, K.W. Kafitz, A. Konnerth, Truncated TrkB-T1 mediates neurotrophin-evoked calcium signalling in glia cells, Nature 426 (2003) 74–78.
[19] Y. Takai, T. Sasaki, T. Matozaki, Small GTP-binding proteins, Physiol. Rev. 81 (2001) 153–208.
[20] X.D. Ren, W.B. Kiosses, M.A. Schwartz, Regulation of the small GTP-binding protein Rho by cell adhesion and the cytoskeleton, EMBO J. 18 (1999) 578–585.
[21] K. Ohira, M. Hayashi, Expression of TrkB subtypes in the adult monkey cerebellar cortex, J. Chem. Neuroanat. 25 (2003) 175–183.
[22] K. Ohira, N. Funatsu, S. Nakamura, M. Hayashi, Expression of BDNF and TrkB receptor subtypes in the postnatal developing Purkinje cells of monkey cerebellum, Gene Expr. Patterns 4 (2004) 257–261.
[23] H. Hirai, P.T. LoVerde, FISH techniques for constructing physical maps on schistosome chromosomes, Parasitol. Today 11 (1995) 310–314.
[24] M.P. Armanini, S.B. McMahon, J. Sutherland, D.L. Shelton, H.S. Phillips, Truncated and catalytic isoforms of trkB are co-expressed in neurons of rat and mouse CNS, Eur. J. Neurosci. 7 (1995) 1403–1409.
[25] S. Yoshimura, H. Sakai, S. Nakashima, Y. Nozawa, J. Shinoda, N. Sakai, H. Yamada, Differential expression of Rho family GTP-binding proteins and protein kinase C isozymes during C6 glial cell differentiation, Mol. Brain Res. 45 (1997) 90–98.
[26] M. Maekawa, T. Ishizaki, S. Boku, N. Watanabe, A. Fujita, A. Iwamatsu, T. Obinata, K. Ohashi, K. Mizuno, S. Narumiya, Signaling from Rho to the actin cytoskeleton through protein kinases ROCK and LIM-kinase, Science 285 (1999) 895–898.
[27] A.L. Bishop, A. Hall, Rho GTPases and their effector proteins, Biochem. J. 348 (2000) 241–255.
[28] T. Yamashita, M. Tohyama, The p75 receptor acts as a displacement factor that releases Rho from Rho-GDI, Nat. Neurosci. 6 (2003) 436–461.
[29] P.A. Barker, E.M. Shooter, Disruption of NGF binding to the low affinity neurotrophin receptor p75LNTR reduces NGF binding to TrkA on PC12 cells, Neuron 13 (1994) 203–215.
[30] S. Etienne-Manneville, A. Hall, Rho GTPases in cell biology, Nature 420 (2002) 629–635.
[31] J. Ng, L. Luo, Rho GTPases regulate axon growth through convergent and divergent signaling pathways, Neuron 44 (2004) 779–793.
[32] J.A. Frost, H. Steen, P. Shapiro, T. Lewis, N. Ahn, P.E. Shaw, M.H. Cobb, Cross-cascade activation of ERKs and ternary complex factors by Rho family proteins, EMBO J. 21 (1997) 6426–6438.
[33] A.J. King, H. Sun, B. Diaz, D. Barnard, W. Miao, S. Bagrodia, M.S. Marshall, The protein kinase Pak3 positively regulates Raf-1 activity through phosphorylation of serine 338, Nature 396 (1998) 180–183.
[34] A. Clerk, F.H. Pham, S.J. Fuller, E. Sahai, K. Aktories, R. Marais, C. Marshall, P.H. Sugden, Regulation of mitogen-activated protein kinases in cardiac myocytes through the small G protein Rac1, Mol. Cell. Biol. 21 (2001) 1173–1184.
[35] H. Bito, T. Furuyashiki, H. Ishihara, Y. Shibasaki, K. Ohashi, K. Mizuno, M. Maekawa, T. Ishizaki, S. Narumiya, A critical role for a Rho-associated kinase, p160ROCK, in determining axon outgrowth in mammalian CNS neurons, Neuron 26 (2000) 431–441.
[36] E. Manser, H.Y. Huang, T.H. Loo, X.Q. Chen, J.M. Dong, T. Leung, L. Lim, Expression of constitutively active alpha-PAK reveals effects of the kinase on actin and focal complexes, Mol. Cell. Biol. 17 (1997) 1129–1143.

Ubiquitin C-terminal hydrolase L1 regulates the morphology of neural progenitor cells and modulates their differentiation

Mikako Sakurai[1,2], Koichi Ayukawa[1], Rieko Setsuie[1,2], Kaori Nishikawa[1], Yoko Hara[1], Hiroki Ohashi[1,3], Mika Nishimoto[1,4], Toshiaki Abe[3], Yoshihisa Kudo[4], Masayuki Sekiguchi[1], Yae Sato[1,2], Shunsuke Aoki[1], Mami Noda[2] and Keiji Wada[1,*]

[1]Department of Degenerative Neurological Diseases, National Institute of Neuroscience, National Center of Neurology and Psychiatry, Kodaira, Tokyo, 187-8502, Japan
[2]Laboratory of Pathophysiology, Graduate School of Pharmaceutical Sciences, Kyushu University, Higashi-ku, Fukuoka, 812-8582, Japan
[3]Department of Neurosurgery, Graduate School of Medicine, Jikei University School of Medicine, Minato-ku, Tokyo, 105-8461, Japan
[4]Laboratory of Cellular Neurobiology, Tokyo University of Pharmacy and Life Science, Hachioji, Tokyo, 192-0392, Japan
*Author for correspondence (e-mail: wada@ncnp.go.jp)

Accepted 27 September 2005
Journal of Cell Science 119, 162-171 Published by The Company of Biologists 2006
doi:10.1242/jcs.02716

Summary

Ubiquitin C-terminal hydrolase L1 (UCH-L1) is a component of the ubiquitin system, which has a fundamental role in regulating various biological activities. However, the functional role of the ubiquitin system in neurogenesis is not known. Here we show that UCH-L1 regulates the morphology of neural progenitor cells (NPCs) and mediates neurogenesis. UCH-L1 was expressed in cultured NPCs as well as in embryonic brain. Its expression pattern in the ventricular zone (VZ) changed between embryonic day (E) 14 and E16, which corresponds to the transition from neurogenesis to gliogenesis. At E14, UCH-L1 was highly expressed in the ventricular zone, where neurogenesis actively occurs; whereas its expression was prominent in the cortical plate at E16. UCH-L1 was very weakly detected in the VZ at E16, which corresponds to the start of gliogenesis. In cultured proliferating NPCs, UCH-L1 was co-expressed with nestin, a marker of undifferentiated cells. In differentiating cells, UCH-L1 was highly co-expressed with the early neuronal marker TuJ1. Furthermore, when UCH-L1 was induced in nestin-positive progenitor cells, the number and length of cellular processes of the progenitors decreased, suggesting that the progenitor cells were differentiating. In addition, NPCs derived from *gad* (UCH-L1-deficient) mice had longer processes compared with controls. The ability of UCH-L1 to regulate the morphology of nestin-positive progenitors was dependent on its binding affinity for ubiquitin but not on hydrolase activity; this result was also confirmed using *gad*-mouse-derived NPCs. These results suggest that UCH-L1 spatially mediates and enhances neurogenesis in the embryonic brain by regulating progenitor cell morphology.

Key words: PGP9.5, UCH-L1, Nestin, Ubiquitin, Cell morphology, Differentiation, Progenitor

Introduction

Ubiquitin C-terminal hydrolase L1 (UCH-L1) is a member of the deubiquitylating enzymes and is one of the most abundant proteins in the brain. Whereas other UCH members are ubiquitously expressed, UCH-L1 is selectively expressed in neurons and testes/ovaries in the adult (Wilkinson et al., 1989). UCH-L1 is also known as PGP9.5 and is used as a neuron-specific marker in neuroanatomical and neuropathological studies (Dickson et al., 1994; McQuaid et al., 1995). Recent studies suggest that UCH-L1 is involved in neurodegeneration. The I93M mutation and the S18Y polymorphism in UCH-L1 are implicated in Parkinson's disease (Leroy et al., 1998; Satoh and Kuroda, 2001). Using gracile axonal dystrophy (*gad*) mice, we previously demonstrated that the dying-back type of axonal degeneration is caused by a deletion of the *Uchl1* gene (Saigoh et al., 1999). UCH-L1 has an affinity for ubiquitin and ensures its stability within neurons in vivo (Osaka et al., 2003). Furthermore, UCH-L1 has ubiquitin ligase activity (Liu et al., 2002). Thus, UCH-L1 might have multiple functions and more roles in biological phenomena than previously expected.

UCH-L1 mRNA is first detected at embryonic day (E) 8.5-9 in the neural tube and in the neural epithelium (Schofield et al., 1995). In addition, UCH-L1 immunoreactivity has been observed in the neural tube at E10.5 (Sekiguchi et al., 2003). However, its functional role in embryonic neurogenesis is not well understood. CDK5 and Dab1 are involved in regulating the migratory behavior of postmitotic neurons. Both p35, which is a CDK5 kinase, and Dab1 are degraded by the ubiquitin-proteasome pathway (Arnaud et al., 2003; Bock et al., 2004; Patrick et al., 1998). Thus, the ubiquitin system might be important in the migration and differentiation of postmitotic neurons and for the lamination pattern of the cerebral cortex.

Neural progenitor cells (NPCs) differentiate into neurons, astrocytes and oligodendrocytes (Qian et al., 1998; Qian et al., 2000; Shen et al., 1998). In the embryonic brain, neuroepithelial cells and radial glia are present in the ventricular zone (VZ); neurogenesis occurs first, followed by

gliogenesis. Committed progenitor cells move from the VZ to the cortical plate (CP) (Noctor et al., 2004). The differentiating cells migrate by means of radial migration, during which the migrating cells change their morphology (Kawauchi et al., 2003; Noctor et al., 2002; Tabata and Nakajima, 2003). Here, we analyzed the functional role of UCH-L1 using mouse embryonic NPCs. Our results indicate that UCH-L1 is expressed in nestin-positive NPCs and might regulate neurogenesis. The expression pattern of UCH-L1 changed in parallel with the transition from neuronal generation to glial generation. Furthermore, UCH-L1 modulated the length of nestin-positive processes in NPCs. Our results constitute the first evidence that UCH-L1 is important in neurogenesis and thus provide the basis for further investigation into the role of the ubiquitin system in neurogenesis.

Results

UCH-L1 expression in embryonic mouse brain

We first determined the specificity of the UCH-L1 antibody using immunoblotting (data not shown) and immunostaining. Because *gad* mice do not express endogenous UCH-L1 (Saigoh et al., 1999), we used these mice as a negative control. Heterozygous littermates had UCH-L1 immunostaining, whereas UCH-L1 immunoreactivity was not detected in the brains of *gad* mice (Fig. 1). These results confirmed the specificity of the antibody against UCH-L1. Using this antibody, we further compared the distribution and expression of UCH-L1 with the neural progenitor marker nestin and the early neuronal marker TuJ1. Nestin was expressed in the VZ of brains from both *gad* and heterozygous mice at E13 (Fig. 1). Nestin expression was observed throughout the region, whereas TuJ1 immunoreactivity was detected at the marginal zone (MZ). In heterozygous mice, UCH-L1 and nestin immunostaining overlapped in almost all cells in the VZ, suggesting that UCH-L1 is expressed in NPCs (Fig. 1A). TuJ1 expression colocalized with that of UCH-L1 in MZ cells, indicating that UCH-L1 is expressed in embryonic neurons as well (Fig. 1B). In E13 *gad* mouse brain, nestin staining differed compared with that in heterozygous littermates. Nestin staining was observed in many long radial fibers in the mutant, which we believed were radial glia; by contrast, staining in the heterozygotes occurred in radial glia as well as in neuronal cells at various stages of development (Fig. 1A; arrow and arrowhead).

We then looked for developmental changes in UCH-L1 expression. In the embryonic cerebral cortex, asymmetric cell division generates one neuron and one neural progenitor (Roegiers and Jan, 2004; Zhong et al., 1996; Zhong et al., 1997). These asymmetric cell divisions begin at E11, peak around E14, and subside after E16. At E14, astrocytes and oligodendrocytes are not yet present. However, at E16, glial cell production begins. The regional expression level for both nestin and TuJ1 did not change between E14 and E16 (Fig. 2A,B). At E14 and E16, nestin immunoreactivity was stronger in the VZ (Fig. 2A) and was faintly detected only along radial glial fibers in the CP (Fig. 2A,C; arrowhead) (Malatesta et al., 2003; Malatesta et al., 2000). TuJ1 immunoreactivity was predominantly detected in the MZ, CP, intermediate zone and subventricular zone at E14 and E16 (Fig. 2B,D). In the VZ, TuJ1 immunoreactivity was detected only in migrating neurons (Fig. 2D; arrowhead).

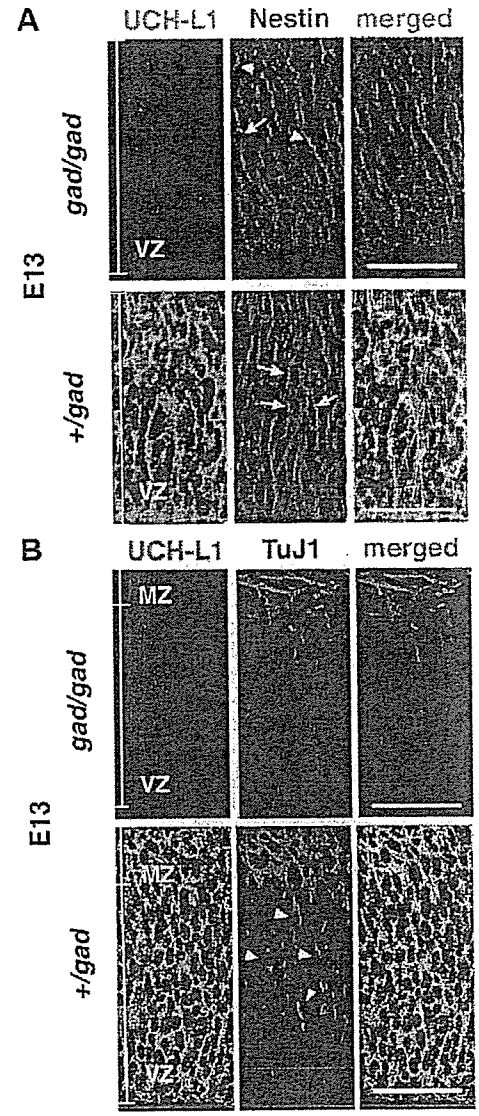

Fig. 1. Antibody specificity and expression of UCH-L1 in the ventricular zone at E13. UCH-L1 expression was detected using immunohistochemistry with anti-PGP9.5. UCH-L1 is not detected in the brain of *gad* mice at E13 (A,B) but is strongly expressed in heterozygous littermates (A,B). Confocal microscopic images of coronal sections of *gad* mice and heterozygous littermates were double stained with antibodies for the progenitor marker nestin and UCH-L1 (PGP9.5) (A) or for the early neuronal marker tubulin β III (TuJ1) and UCH-L1 (B). Long radial fibers are indicated by arrowheads, and various phases of progenitor cells are indicated by arrows (A). TuJ1-positive, migrating neuronal cells are indicated by arrowheads (B). MZ, marginal zone; VZ, ventricular zone. Bars, 40 μm.

By contrast, the pattern of UCH-L1 expression changed between E14 and E16 (Fig. 2A,B). At both stages of development, UCH-L1 was expressed in neuronal cells as well as in progenitor cells. UCH-L1 immunoreactivity was stronger in the VZ than in the CP at E14; however, the immunoreactivity

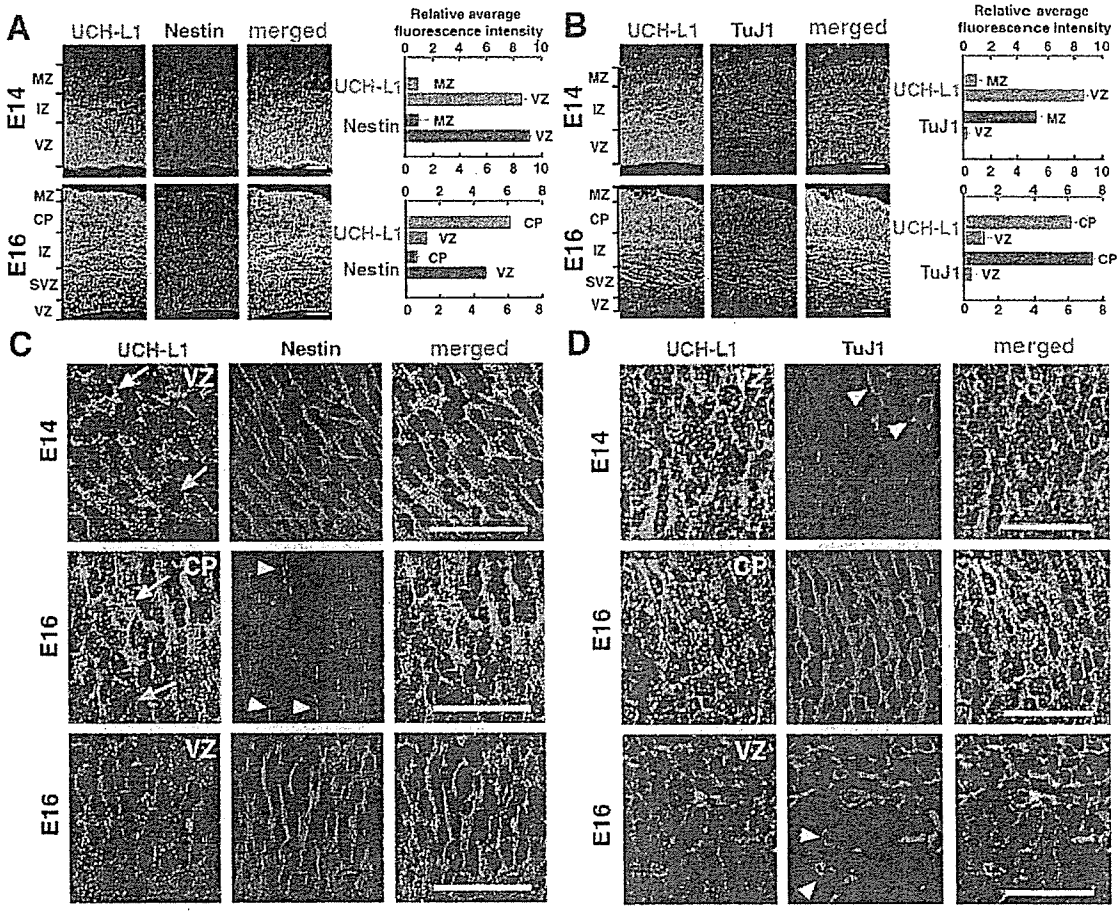

Fig. 2. Change in UCH-L1 expression pattern in the developing mouse brain. Cryosections of the brain at E14 and E16 were double stained with UCH-L1 and the neural progenitor marker nestin (A) or early neuronal marker TuJ1 (B). Unlike with UCH-L1, staining patterns for TuJ1 and nestin do not change between E14 and E16. At E14, UCH-L1 expression is higher in the VZ than in the MZ. At E16, higher expression of UCH-L1 is reciprocally detected in the CP. By contrast, at both E14 and E16, nestin is highly expressed in the VZ, and TuJ1 expression is higher in the MZ/CP. Fluorescence intensities per field (1700 μm^2) were measured in each layer of the E14 and E16 brain and are shown to the right. Bars, 80 μm. (C,D) Higher-magnification images from A,B of UCH-L1 expression in the E14 and E16 brain: UCH-L1 and nestin (C); UCH-L1 and TuJ1 (D). UCH-L1 and nestin are co-expressed in the VZ at E14 and E16. Nestin is expressed only in radial glial fibers (arrowheads) of the CP but not in neurons. UCH-L1 expression level is high. A representative cell with a high level of UCH-LI expression is indicated by a white arrow and one with low expression is indicated by a yellow arrow (C). An early neuronal marker, TuJ1, was expressed in both migrating (arrowheads) and mature neurons (D). CP, cortical plate; IZ, intermediate zone; MZ, marginal zone; SVZ, subventricular zone; VZ, ventricular zone. Bars, 40 μm.

was stronger in the CP than in the VZ at E16 (Fig. 2A,B). The regional change in UCH-L1 expression between E14 and E16 was further confirmed by measuring immunofluorescence intensities from confocal images of the MZ/CP and VZ. At E14, the relative UCH-L1 expression level in the VZ was 9.3 times higher than that in the MZ (Fig. 2A).

Conversely, at E16, when neuronal maturation occurs in the CP, UCH-L1 immunoreactivity in the CP was 5.0 times higher than in the VZ (Fig. 2B). UCH-L1 immunoreactivity colocalized with that of nestin in the VZ at both E14 and E16, although UCH-L1 expression in the VZ was lower at E16 (Fig. 2C). In the VZ at E14, nestin was expressed homogeneously; however, the pattern of UCH-L1 immunoreactivity was mixed, with strong and weak intensities (Fig. 2C; arrow). This expression pattern might reflect the heterogeneity of progenitor cells. Nestin-positive radial glial fibers were observed in the CP at E16 through mature neurons, which strongly expressed UCH-L1 (Fig. 2C) (Malatesta et al., 2000; Malatesta et al., 2003).

UCH-L1 and nestin expression in cultured NPCs

Because areas of nestin and UCH-L1 immunoreactivity overlapped in the VZ, where NPCs reside, we subsequently analyzed the transition of UCH-L1 expression using cultured NPCs. We performed double-labeling experiments for UCH-L1 and nestin expression in cultured NPCs. In the presence of basic fibroblast growth factor (bFGF), when NPCs are proliferating, the percentage of UCH-L1/nestin double-positive

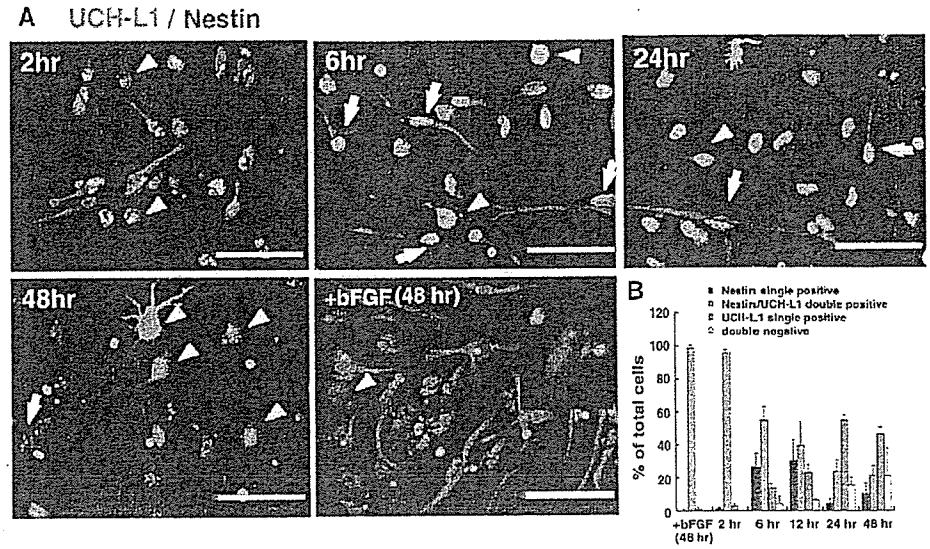

Fig. 3. Nestin and UCH-L1 expression in undifferentiated and differentiating NPCs at 2, 6, 12, 24 and 48 hours. (A) NPCs were immunolabeled with antibodies against nestin and UCH-L1 in the proliferating phase (+bFGF; at 48 hours) or the differentiation phase (–bFGF; 2, 6, 24, 48 hours). Cultures were counterlabeled with Hoechst nuclear dye to facilitate cell quantification. (B) Quantitative analysis of the percentage of cells stained with each antibody. Nestin-positive cells gradually decrease as differentiation proceeds. The UCH-L1 expression level is both high (arrowheads) and low (arrows) in nestin-positive cells at 6 hours. Each experiment was analyzed by counting cells in three independent wells at the indicated times. The experiments were repeated at least two times. Bars, 50 μm.

cells did not change 48 hours after plating, and almost all NPCs expressed UCH-L1 (Fig. 3A). The majority (97.5±2.2%; mean±s.d.) of cultured cells were nestin positive and most of them also stained for UCH-L1 2 hours after plating without bFGF, which triggers NPC differentiation. UCH-L1/nestin double-positive cells were detected at all time points, but as differentiation proceeded their numbers gradually decreased from 95.8±1.9% at 2 hours to 21.5±5.8% at 48 hours (Fig. 3A,B). Although UCH-L1 single-positive cells were rarely detected at 2 hours, the population increased with differentiation, and by 24 hours after bFGF removal 55.1±2.9% of cultured cells were UCH-L1 single-positive cells. Conversely, nestin single-positive cells were readily detected during the earlier phase of differentiation, especially at 6 hours (26.4±8.4% of total cells) and 12 hours (27.0±14.0% of total cells). The differentiating NPCs included nestin-positive cells in which UCH-L1 was either strongly or weakly expressed (Fig. 3A; arrow and arrowhead at 6 hours). These data indicate that UCH-L1 is expressed in progenitor cells as well as in differentiating NPCs. Nestin-positive cells can probably be

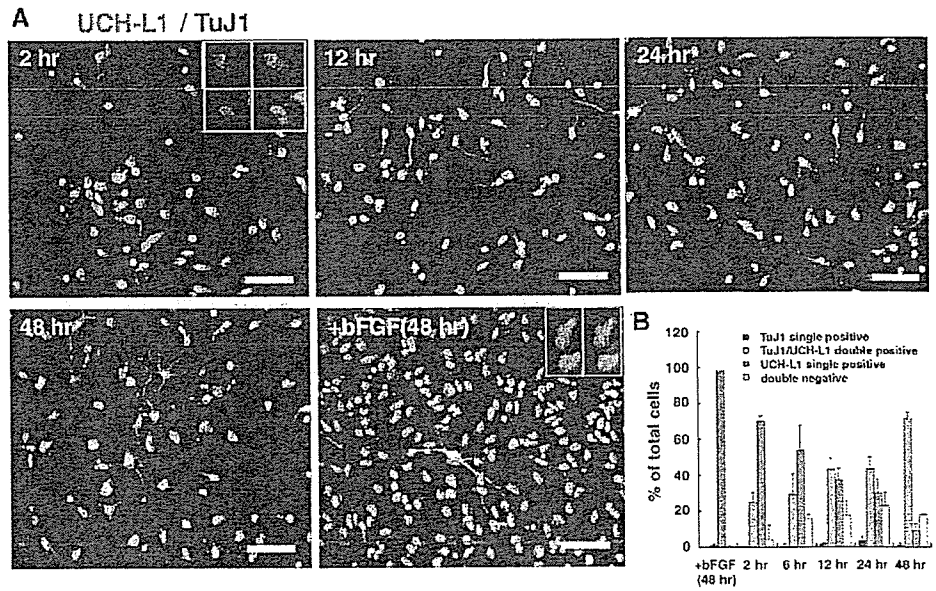

Fig. 4. UCH-L1 expression in neurogenesis. NPCs were immunolabeled with antibodies against TuJ1 and UCH-L1. Cultures were counterlabeled with Hoechst nuclear dye to facilitate cell quantification. Quantitative analysis of the percentage of cells stained with each antibody. (A) In the proliferating phase (+bFGF; at 48 hours) or the differentiation phase (–bFGF; 2, 12, 24, 48 hours), most TuJ1-positive cells co-express UCH-L1. The UCH-L1 expression level is both high and low in TuJ1-positive cells at 48 hours. (B) Quantitative analysis of the percentage of cells stained with each antibody. The number of TuJ1-positive cells gradually increased in the differentiating phase (–bFGF; B). Each experiment was analyzed by counting cells in three independent wells at the indicated times. The experiments were repeated at least two times. Bars, 50 μm.

categorized into at least two subgroups based on their UCH-L1 expression (Fig. 3A,B).

UCH-L1 and TuJ1 expression in cultured NPCs

We then analyzed the expression patterns of UCH-L1 and TuJ1. In the presence of bFGF, TuJ1-positive cells were rarely detected. However, in the absence of bFGF, TuJ1-positive cells were induced. In the cultures without bFGF, as the UCH-L1 single-positive cell population decreased with time, the UCH-L1/TuJ1 double-positive population increased (Fig. 4A,B). UCH-L1/TuJ1 double-negative cells were detected in the differentiating phases at 6, 12, 24 and 48 hours. UCH-L1/TuJ1 double-negative cells might be the nestin single-positive cells at 6 hours and 12 hours in Figs 3 and 4. TuJ1 single-positive cells were infrequently detected in the differentiating NPCs. Because 71.4±3.4% of NPCs differentiated into TuJ1-positive cells under our culture conditions without bFGF at 48 hours, almost all UCH-L1-positive cells are thought to differentiate into TuJ1-positive neuronal cells (Fig. 4A,B). The differentiating NPCs included TuJ1-positive cells in which UCH-L1 was either strongly or weakly expressed (Fig. 4A). These data indicate that UCH-L1-positive NPCs have a high potential for differentiating into neuronal cells and that TuJ1-positive neuronal cells are heterogeneous with regard to UCH-L1 expression.

Morphological classification of UCH-L1-positive NPCs

Nestin is a marker of undifferentiated cells, whereas UCH-L1 is a neuron-specific marker. Here, UCH-L1/nestin double-positive cells were present in cultured NPCs as well as in embryonic brain (Figs 2, 3). Cultured NPCs sequentially gave rise to neurons, then astrocytes, and finally oligodendrocytes (data not shown). Under our culture conditions, neurogenesis actively occurred in differentiating NPCs between 2 and 12 hours after plating (Fig. 4). Glial differentiation had not begun by this time. We collected differentiating NPCs at 6 hours and 12 hours after plating and then analyzed the morphology of nestin-positive cells (Fig. 5). Both UCH-L1/nestin double-positive cells and nestin single-positive cells were present in the population of differentiating NPCs. As the population of double-positive cells might represent a progression of differentiating neurons, we examined the morphology of these cells. Differentiating neurons undergo a stereotypical set of morphological changes, including length (from long to short) (Fukuda et al., 2003; Hartfuss et al., 2003; Nadarajah et al., 2001). We categorized the nestin-positive cells with respect to process length (long, short or round; Fig. 3). UCH-L1 single-positive and double-negative cells were included in the total number of cells. When the total length of processes was more than four times the diameter of the nucleus of the cell, the cell was categorized as 'long', whereas cells with shorter processes were categorized as 'short'. Cells that did not have processes were classified as 'round'. At 6 hours, the majority of nestin single-positive cells were long (18.2±7.6% vs 4.0±0.2% short cells; mean±s.d.; Fisher's PLSD, P=0.008), whereas the majority of UCH-L1/nestin double-positive cells were short (62.0±6.3%). This population was significantly greater than that of long cells (10.3±2.0%) and round cells (5.0±1.7%; Fisher's PLSD, P<0.0001). When NPCs with processes were subcategorized as unipolar, bipolar or multipolar, the unipolar population was significantly higher (62.3±16.9%) than the bipolar population (18.2±3.9%; Fisher's PLSD, P=0.002) in UCH-L1/nestin double-positive cells. Multipolar cells were not observed at 12 hours. However, in nestin single-positive cells, more NPCs were bipolar (16.5±4.6%) than unipolar (4.5±1.9%; Fisher's PLSD, P=0.009; Fig. 6B). Similar results were obtained at 12 hours (Fig. 6). Thus, most UCH-L1/nestin double-positive cells had shorter processes and were more likely to be unipolar.

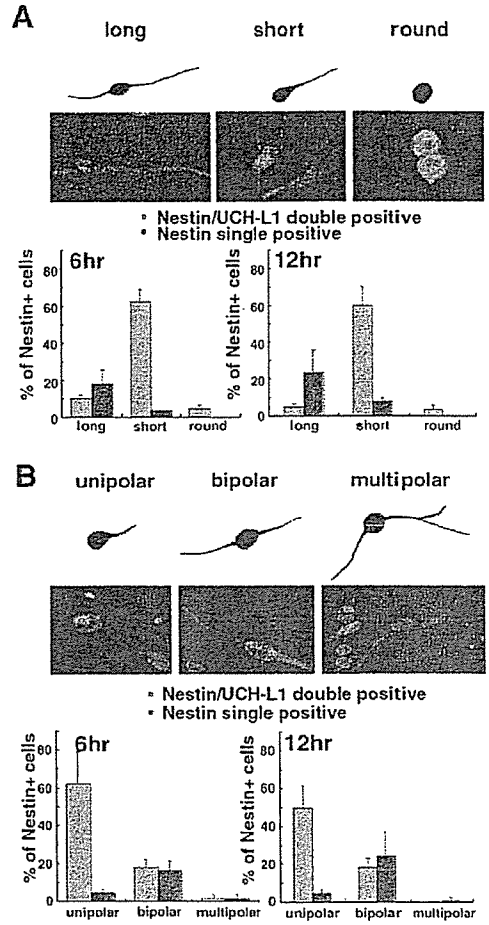

Fig. 5. Morphological identification of subpopulations of cultured NPCs at 6 and 12 hours after induction of differentiation. Differentiating NPCs were double stained with UCH-L1 and nestin. For the quantification depicted in A, differentiating NPCs stained with UCH-L1 and nestin were classified as long, short or round (see text). For the quantification depicted in B, differentiating NPCs were classified based on three kinds of cell morphology: unipolar, bipolar, or multipolar.

Effect of UCH-L1 on nestin-positive processes

We next examined the effect of UCH-L1 on proliferating NPC morphology using the transient transfection method. NPCs were allowed to proliferate for 48 hours after transfection and were then induced to differentiate for 12 hours. The cells were fixed, and the length of nestin-positive processes was examined. To quantify the relationship between UCH-L1 expression and process formation, we measured the total length

of nestin-positive processes. Untransfected NPCs that were nestin positive had mainly long, bipolar processes (Fig. 3A, +bFGF). Cells that were transfected with a green fluorescent protein (GFP) expression vector (negative control) had a morphology that was similar to that of untransfected cells (Fig. 6A). By contrast, cells transfected with wild-type (WT) UCH-L1 cDNA had significantly shorter processes (47.6±6.4 μm, mean±s.e.m., n=81) than mock-transfected cells (69.9±7.0 μm, n=82) (Fig. 6A).

We then examined the relationship between the UCH-L1 structure and its activity with respect to morphological induction. We prepared two UCH-L1 mutants: D30A UCH-L1 lacked hydrolase activity and binding affinity for ubiquitin (Fig. 6B,C) (Osaka et al., 2003); C90S UCH-L1 lacked hydrolase activity but maintained binding affinity for ubiquitin (Fig. 6B,C) (Osaka et al., 2003). We compared the deubiquitylating activity of each UCH-L1 mutant using Ub-AMC as a substrate. The D30A mutant had little hydrolase activity, and the activity of the C90S mutant was not detectable (Fig. 6B; right). Sodium dodecyl sulfate-polyacrylamide gel electrophoresis revealed that there were no detectable contaminating proteins in these recombinant protein preparations (Fig. 6B; left). Co-immunoprecipitation experiments demonstrated that WT UCH-L1 and the C90S mutant physically associated with monoubiquitin. The D30A mutant (as well as GFP alone, which was used as a control) did not associate with ubiquitin (Fig. 6C). Although we did not detect a statistically significant difference, cells transfected with the D30A mutant tended to have longer nestin-positive processes (83.4±7.1 μm, n=87) as compared with cells transfected with the GFP expression vector (Fig. 6A). By contrast, cells transfected with the C90S mutant had significantly shorter fibers (39.3±4.5 μm, n=120; ANOVA: F=11.5, P<0.0001; Dunnett's multiple comparison test: GFP vs WT, P<0.05; GFP vs C90S, P<0.001; GFP vs D30A, P>0.05; Fig. 6A). We also compared the length of nestin-positive processes among UCH-L1 mutants (Bonferroni-Dunn Multiple Comparison Test: WT vs C90S, P=0.32; WT vs D30A, P<0.0001; D30A vs C90S, P<0.0001). Taken together, our data suggest that the effect of UCH-L1 expression on NPC morphology is dependent on the interaction between monoubiquitin and UCH-L1.

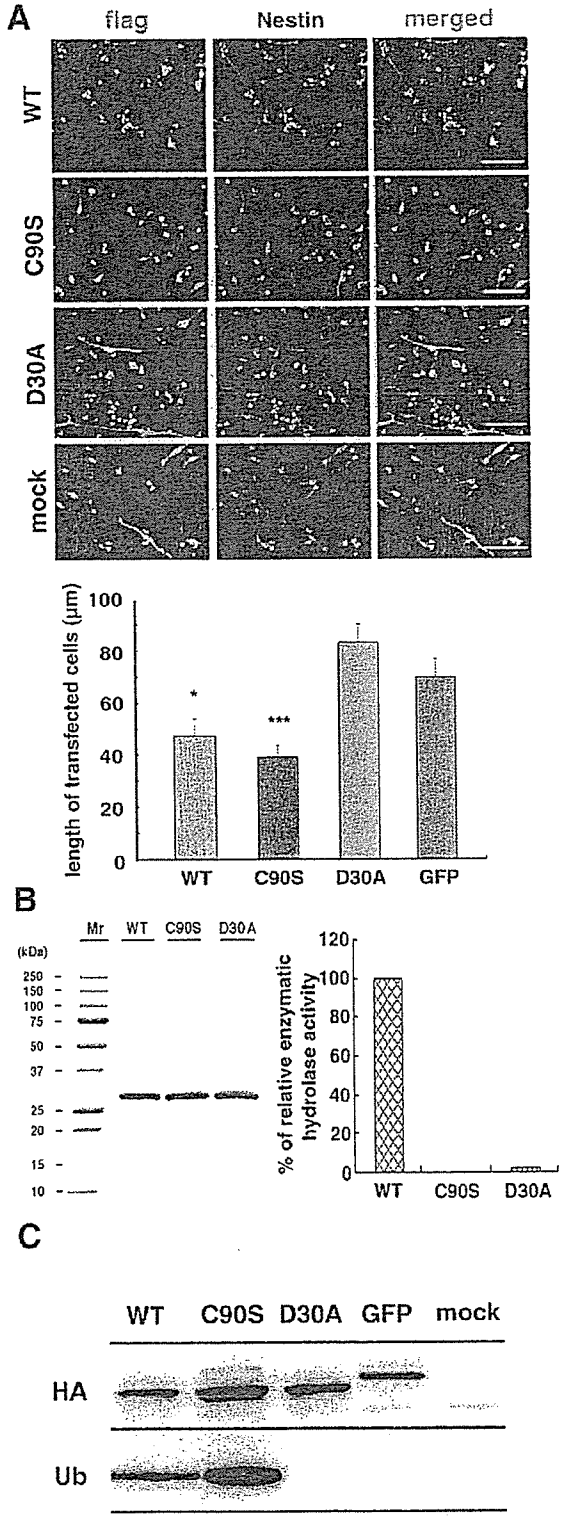

Fig. 6. The induction of short processes depends on the interaction between UCH-L1 and monoubiquitin. (A) FLAG-tagged WT UCH-L1, C90S UCH-L1, D30A UCH-L1 and GFP (all in the pCI-*neo* vector) were transfected into NPCs. Antibodies against the FLAG-tag were used to detect transfected UCH-L1. The green staining shows transfected cells and the red staining shows endogenous nestin. Transient transfection of each construct was performed under proliferating conditions. At 48 hours after transfection, bFGF was removed for 12 hours before the cultures were immunostained. The lengths of nestin-positive processes in immunostained cells were measured. Asterisks indicate differences from the value of GFP-transfected NPCs at *P<0.05 and ***P<0.001. Bars, 80 μm. (B) Visualization of recombinant 6HN-tagged UCH-L1 by sodium dodecyl sulfate-polyacrylamide gel electrophoresis with Coomassie staining (B, left). UCH-L1 hydrolase activity was measured by Ub-AMC hydrolysis. Enzyme concentration was 4.3 nM, and substrate concentration was 700 nM. Initial velocity data was used to determine the values for relative hydrolase activity of UCH-L1 (B, right). (C) UCH-L1 co-immunoprecipitated with Ub. Cytosolic extracts from NIH-3T3 cell lines stably expressing HA-tagged WT UCH-L1 and mutants thereof were immunoprecipitated using anti-HA and immunoblotted with anti-HA antibody or anti-Ub antibody.

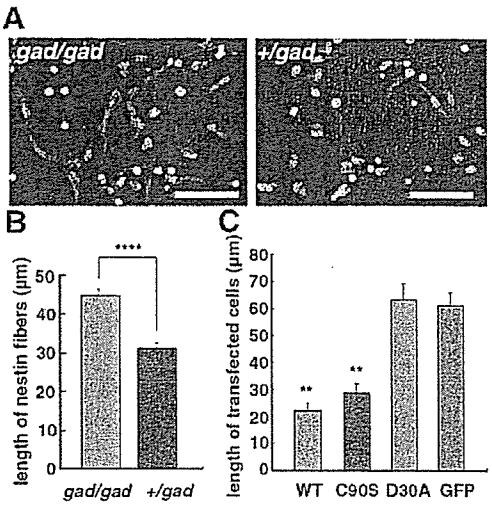

Fig. 7. A comparative experiment of *gad* mice and heterozygous littermates. The experiment compared *gad* mice (A,B) with a transfection study using FLAG-tagged WT UCH-L1, C90S UCH-L1, D30A UCH-L1 and GFP (mock) into *gad*-mouse-derived NPCs (C). The lengths of nestin-positive processes in immunostained cells were measured. NPCs from *gad* mice had longer nestin-positive processes compared with the control (A,B). (C) At 48 hours after transfection, bFGF was removed for 12 hours before the cultures were immunostained. The lengths of nestin-positive processes in immunostained cells were measured. Asterisks indicate differences from the value of GFP-transfected NPCs at $^{**}P<0.01$ and $^{****}P<0.0001$. Bar, 50 μm.

A comparative experiment using *gad*-mouse-derived NPCs

We did a comparative experiment using *gad* mice and heterozygous littermates. Nestin-positive NPCs from *gad* mice had longer processes. When we measured the length of nestin-positive fibers, NPCs from *gad* mice (45.0±1.4 μm, mean±s.e.m., n=366) had significantly longer nestin-positive processes compared with the control (31.4±1.3 μm, n=363) (Mann-Whitney U test: *gad* vs control, $P<0.0001$; Fig. 7A,B).

We next examined the effect of UCH-L1 on *gad*-mouse-derived NPCs using the transient transfection method. As observed in B6-derived cells, NPCs from *gad* mice that were transfected with WT UCH-L1 cDNA had significantly shorter processes (22.2±2.7 μm, mean±s.e.m., n=70) than mock-transfected cells (61.0±4.9 μm, n=88) (Bonferroni-Dunn multiple comparison test: GFP vs WT, $P<0.0001$) (Fig. 7C). Similarly, cells transfected with the C90S mutant had significantly shorter fibers (28.9±3.1 μm, n=71) (GFP vs C90S, $P<0.0001$). Although we did not detect a statistically significant difference, cells transfected with the D30A mutant tended to have longer nestin-positive processes (63.3±5.9 μm, n=80) as compared with cells transfected with the GFP expression vector (GFP vs D30A, P=0.70) (Fig. 7C). We also compared the length of nestin-positive processes among UCH-L1 mutants (Bonferroni-Dunn multiple comparison test: WT vs C90S, P=0.32; WT vs D30A, $P<0.0001$; D30A vs C90S, $P<0.0001$). Taken together, our data suggest that the effect of UCH-L1 expression on NPC morphology is dependent on the interaction between monoubiquitin and UCH-L1.

Discussion

UCH-L1 is a neuron-specific marker in the adult brain. In the present study, we provide experimental evidence that UCH-L1 is expressed in NPCs (Figs 2, 3). Using immunohistochemistry in the mouse brain, we detected UCH-L1 expression at E14 and E16. Interestingly, the expression pattern differed between E14 and E16 (Fig. 2). At E14, when the CP is forming, UCH-L1 expression was higher in the VZ than in the CP. At E14, the VZ contains progenitor cells that are generating neurons in the neocortex (Hashimoto and Mikoshiba, 2004; Malatesta et al., 2003). By contrast, UCH-L1 expression at E16 was lower in the VZ than in the CP. At E16, neuritogenesis and neuronal maturation are active in the CP, and gliogenesis is beginning in the VZ (Rice and Curran, 2001). The cerebral cortex layer becomes thicker at E16, where glial cells are not yet generated. The staining pattern for TuJ1 and nestin did not change between E14 and E16 (Fig. 2), indicating that UCH-L1 is highly expressed in the cortical layer prior to gliogenesis. The change in the expression pattern of UCH-L1 was coincident with the transition from neurogenesis to gliogenesis in the VZ. These results raise the possibility that UCH-L1 mediates not only the neuronal differentiation of NPCs but also the transition from neurogenesis to gliogenesis.

Time is a pivotal factor in the programmed sequence that produces neurons and glial cells from NPCs (Qian et al., 2000), in that the switch from neurogenesis to gliogenesis is regulated by time. The mechanism behind this progression of the progenitor cells is not well understood. Cultured NPCs generate neurons first, followed by astrocytes and then oligodendrocytes (Qian et al., 2000; Temple, 2001). This order of production for each population has been verified in vivo (Sauvageot and Stiles, 2002). The pattern of UCH-L1 immunoreactivity suggests that UCH-L1 is required for the onset of neurogenesis, which is followed by glial differentiation (Fig. 2).

We thus examined the role of UCH-L1 in neurogenesis using cultured NPCs. In UCH-L1/nestin double-staining experiments, the number of double-positive cells decreased with time in culture (Fig. 3). Conversely, UCH-L1 single-positive cells increased. In the double-staining experiments for UCH-L1 and TuJ1, the number of UCH-L1 single-positive cells decreased with time in culture, whereas the number of UCH-L1/TuJ1 double-positive cells increased (Fig. 4). These observations suggest that most UCH-L1-positive cells initially express nestin, but they express TuJ1 at a later stage. As we observed in vivo and in vitro (Figs 2-4), NPCs express UCH-L1, and its expression increases as the NPCs differentiate into neuronal cells. The number of nestin single-positive cells transiently increased before the UCH-L1 single-positive population increased (Fig. 3). The nestin single-positive population might have changed into the UCH-L1/nestin double-negative population (Fig. 3). Although the fate of the double-negative populations remains unknown, the double-negative cells might represent glial cells. Alternatively, some of the nestin single-positive cells might have changed into UCH-L1/nestin double-positive cells and then differentiated into UCH-L1 single-positive cells. A few UCH-L1-negative and TuJ1-positive cells were detected in the differentiating NPCs (Fig. 4). Thus, TuJ1-positive early neurons appear to be heterogeneous. UCH-L1/TuJ1 double-positive immunoreactivity suggested that UCH-L1 is not

absolutely required for some portion of neuronal cell development (Fig. 1B and Fig. 4A). This might explain why *gad* mouse neurons develop despite the absence of UCH-L1.

Because UCH-L1 was expressed in nestin-positive NPCs, we further examined the role of UCH-L1 in cell morphology (Fig. 5). Differentiating NPCs change morphology (Noctor et al., 2001), but the role of UCH-L1 in differentiating neurons has not been investigated. We classified nestin-positive cells based on the length of their processes. Nestin single-positive cells were predominantly long, whereas most UCH-L1/nestin double-positive cells were predominantly short (Fig. 5). These results suggest that UCH-L1 plays a role in regulating NPC process length. We examined this possibility by inducing UCH-L1 in nestin-positive cells. Untransfected, proliferating nestin-positive NPCs had mainly long and bipolar processes [Fig. 3A, bFGF (48 hours)], but when UCH-L1 was transfected, the length of nestin-positive NPC processes shortened (Fig. 6A). The unipolar population increased following UCH-L1 expression. These results support the idea that UCH-L1 regulates NPC morphology. This idea was further confirmed by observations in NPCs from *gad* mice; as shown in Fig. 7B, NPCs from homozygous *gad* mice had longer processes than those from heterozygous controls. In addition, we observed that transfection of UCH-L1 shortened the processes of NPCs from *gad* mice compared with mock transfectants (Fig. 7C).

Our results also suggest that at least two populations of NPCs exist in the embryonic brain. The populations can be classified by the presence or absence of UCH-L1. In the dentate gyrus of the adult mouse brain, there are two distinct subpopulations of nestin-positive cells (Fukuda et al., 2003): those having short processes differentiate into neurons, whereas those having long processes generate late progenitors, which have short processes. The nestin staining pattern of brains from *gad* mice differed from that of brains from heterozygous littermates (Fig. 1). In the *gad* mouse brain, nestin-positive radial fibers were prominent, and almost all progenitor cells appeared to have long processes (Fig. 1). Since UCH-L1 affected NPC morphology (Fig. 6A and Fig. 7C), the difference in vivo indicates that differentiation itself was modulated by the absence of UCH-L1. Considering that neurons are present in the *gad* mouse even though it lacks UCH-L1 expression, further investigation into the morphological role of UCH-L1 using various approaches including the BrdU studies should provide important information about the heterogeneity of cortical neurons.

UCHs hydrolyze ubiquitin C-terminal small adducts in vitro (Larsen et al., 1998). Recently, a significant relationship was reported between UCH-L1 hydrolase activity and cell proliferation in lung cancer cell lines (Liu et al., 2003). We previously demonstrated that UCH-L1 extends ubiquitin half-life and prevents ubiquitin degradation. This function depends on the interaction between UCH-L1 and monoubiquitin but not on hydrolase activity (Osaka et al., 2003). In the present study, WT UCH-L1 and the C90S mutant both decreased the length of NPC processes. Both molecules associate with monoubiquitin, unlike another mutant, D30A, which did not affect process length (Fig. 6). Similar results were obtained from the transfection study using nestin-positive NPCs from *gad* mice (Fig. 7C). Thus, the effect of UCH-L1 on NPC process length is dependent on the interaction between UCH-L1 and ubiquitin but not on hydrolase activity. Although we did not examine the ligase activity of each mutant (Liu et al., 2002), the C90S mutant is unlikely to have ligase activity, because conjugation of ubiquitin to the C90S mutant forms a stable complex that prevents the release of ubiquitin (Sullivan and Vierstra, 1993). This observation suggests that the ligase activity is not related to the morphological changes that occurred in NPCs.

The ubiquitin system has an essential role in various physiological events, including cell-cycle progression, specific gene transcription, membrane protein trafficking, reversal of stress damage and intracellular signaling (Weissman, 2001). In cortical neurogenesis, the role of the ubiquitin system is not well understood. Several molecules that are important in cortical neurogenesis, including Notch, P35 and Dab1, are ubiquitylated (Arnaud et al., 2003; Bock et al., 2004; Patrick et al., 1998; Qiu et al., 2000). Here we show for the first time that UCH-L1 is expressed in NPCs and regulates their morphology. In addition, in vivo UCH-L1 expression is localized to the VZ and cortical layers that are undergoing neurogenesis. Cells undergoing gliogenesis had little UCH-L1 expression in vivo. These results suggest that UCH-L1 facilitates neurogenesis, an activity that appears to depend on the affinity of UCH-L1 for ubiquitin.

Materials and Methods

Animals

Pregnant C57BL/6J mice were purchased from CLEA Japan. The *gad* mouse is an autosomal recessive mutant that was obtained by crossing CBA and RFM mice (Saigoh et al., 1999). The *gad* line was maintained by intercrossing for more than 20 generations (Kwon et al., 2003; Saigoh et al., 1999). All animal experiments were performed in the laboratory according to the NIH Standards for Treatment of Laboratory Animals.

Antibodies and reagents

Monoclonal and polyclonal antibodies used in this study were as follows: monoclonal anti-nestin antibody (Becton Dickinson; and Rat401, Developmental Studies Hybridoma Bank, The University of Iowa, Iowa City, IA), monoclonal anti-neuronal tubulin β III antibody (TuJ1; Covance), polyclonal anti-UCH-L1 antibody (PGP9.5; RA95101, UltraClone), and polyclonal anti-FLAG antibody (Sigma). All secondary polyclonal antibodies conjugated to Alexa Fluor fluorescein were purchased from Molecular Probes.

Cortical NPC culture and differentiation conditions in C57BL/6 mice

Cortical NPCs were cultured as previously described (Nakashima et al., 1999). Briefly, embryos were removed from pregnant C57BL/6J mice (CLEA Japan) and staged according to morphological criteria to confirm the gestational day (Kaufman et al., 1998). Developing mouse cerebral cortex was dissected from E14 embryos. Cells were mechanically dissociated by trituration and plated at a concentration of 3.0×10^6 cells per 10 cm dish (Becton Dickinson) precoated with 10 ml of 15 μg/ml poly-L-ornithine (Sigma) and 10 ml of 1 μg/ml fibronectin (Nitta Gelatin). Cells were expanded for 5 days in serum-free neurobasal (NB) medium (Invitrogen) supplemented with B27 (Invitrogen), 0.5 mM L-glutamine (Invitrogen), 100 U/ml penicillin and 100 μg/ml streptomycin (Invitrogen). This medium contained 10 ng/ml bFGF (PeproTech). Cultures were maintained at 37°C in an atmosphere of 95% air and 5% CO_2. For secondary culture, bFGF-expanded NPCs were washed in warm Hank's Balanced Salt Solution, detached with mechanical pipetting, and resuspended in NB medium supplemented with B27, but not bFGF. Cells were then replated in 24-well plates (Nunc; 1.8×10^5 cells per well) that were precoated with 500 μl of 15 μg/ml poly-L-ornithine and 500 μl of 1 μg/ml fibronectin for immunofluorescence staining at each time point.

Cortical NPC culture and differentiation conditions in *gad* mice

Culture of NPCs derived from *gad* mice was performed as with NPCs derived from B6 mice. Developing mouse cerebral cortex was dissected from embryos at E13.5 to E14.5. The precise gestational day was determined according to previously established morphological criteria (Kaufman et al., 1998). NPCs from each embryo were collected and cultured separately. Each genotype was determined later using PCR and, as a result, each pair of *gad* and control littermate mice from two sets of

parents were used. Each culture of NPCs was replated in 24-well plates without bFGF and stained using anti-UCH-L1 24 hours after plating.

Immunohistochemistry

Brain sections were stained as previously described (Li et al., 2003; Osaka et al., 2003). Briefly, E14 and E16 mouse brains were removed and fixed in 4% paraformaldehyde/phosphate-buffered saline (PBS) for 2 hours at room temperature, cryoprotected in 30% sucrose in PBS and frozen in dry ice. Sections (20 μm thick) were cut on a cryostat, and mounted on aminopropylsilane (APS)-coated glass slides. They were then washed three times in PBS for 5 minutes, and blocked for 1 hour at room temperature with 3% bovine serum albumin, 2% (v/v) normal goat serum, and 0.2% (v/v) Triton X-100 in PBS (pH 7.4). Sections were incubated with primary antibodies [anti-nestin antibody (Rat401) 1:10; or anti-UCH-L1 antibody (RA95101) 1:4000; or anti-TuJ1 antibody, 1:1000] overnight at 4°C or for 2 hours at room temperature. After rinsing in PBS, the sections were incubated for 2 hours with diluted fluorescein-conjugated secondary antibody (1:200). The images were obtained with a confocal laser scanning TCS SL microscope, and detailed analyses were performed using an LSC confocal microscope system (Leica). Immunofluorescence intensities were measured from confocal images with Mac SCOPE software (version 2.59; Mitani).

Immunocytochemistry

Cells were stained as previously described (Aoki et al., 2002). Briefly, all incubations and washes were performed at room temperature. Cells were fixed with 3.8% formaldehyde/PBS for 10 minutes and permeabilized with 0.02% (v/v) Triton X-100/PBS for 5 minutes. Fixed cells were blocked with 3.3% goat serum for 30 minutes. Cells were incubated with a diluted primary polyclonal or monoclonal antibody (both were used for double staining) for 0.5-1 hour. The cells were then incubated with diluted secondary antibody conjugated to fluorescein for 0.5-1 hour. Antibody dilutions were as follows: anti-UCH-L1 antibody, 1:4000; anti-nestin antibody, 1:500; anti-TuJ1, 1:500. All secondary antibodies were diluted 1:200 in 1% goat serum/PBS before use. The images were obtained with fluorescence microscopy on an IX70 microscope (Olympus).

Transfection

For C57BL/6 mice, cells replated in 24-well plates were cultured overnight in growth medium containing bFGF and B27. The next day, each construct was transfected using Lipofectamine 2000 (Invitrogen) according to the manufacturer's instructions. NPCs were allowed to proliferate for 48 hours after transfection and then induced to differentiate for 12 hours without bFGF. For *gad*-mouse-derived NPCs, transfection was done in a similar manner.

Expression plasmids for human UCH-L1 variants

Mutant cDNAs encoding human UCH-L1 containing either the D30A or C90S substitution were obtained using the QuikChange site-directed mutagenesis kit (Stratagene) with the following mutagenesis oligonucleotides: 5′-CAGTGG-CGCTTCGTGGCCGTGCTGGGGCTGGAAG-3′ and 5′-CTTCCAGCCCCAG-CACGGCCACGAAGCGCCACTG-3′ for D30A; 5′-CCATTGGGAATTCCTCT-GGCACAATCGGAC-3′ and 5′-GTCCGATTGTGCCACAGGAATTCCCAA-TGG-3′ for C90S. Each single-nucleotide mutation in the resulting plasmids was confirmed by sequencing. Mammalian expression plasmids containing either FLAG-tagged human WT UCH-L1 or the D30A or C90S mutants were constructed using a pCI-*neo* mammalian expression vector (Promega). Bacterial expression plasmids containing either 6HN-tagged human WT UCH-L1 or the D30A or C90S mutants were constructed using a tetracycline-inducible expression system. *Xho*I-*Not*I cDNA fragments of the pCI-*neo* WT UCH-L1 or the D30A and C90S mutants and constructs were digested, and the DNA fragments were ligated between the *Sal*I and *Not*I sites in pPROtetE233 (Clontech) to generate pPROtetE233 6HN-tagged human WT, D30A and C90S UCH-L1 vectors. These expression plasmids were confirmed by sequencing.

In vitro assay for human UCH-L1 activity

Purified human UCH-L1 and the fluorogenic substrate ubiquitin-7-amino-4-methylcoumarin (Ub-AMC; Boston Biochem) were used to determine steady-state kinetic parameters as described previously (Nishikawa et al., 2003).

Immunoprecipitation

NIH-3T3 cells stably expressing human WT UCH-L1 or the C90S or D30A mutants, all with an HA-FLAG double tag at the N terminus, were cultured to subconfluency in a 10 cm dish, lyzed with 1 ml of modified RIPA buffer [50 mM Tris-HCl, pH 7.5, 1% (v/v) NP-40, 0.25% sodium deoxycholate, 150 mM NaCl, 1 mM EDTA] with EDTA-free complete protease inhibitor cocktail (Roche), sonicated and centrifuged at 18,000 *g* for 20 minutes at 4°C. Immunoprecipitation was performed as described previously (Ogawa et al., 2002).

Statistics

Statistical analyses were performed using StatView, version 5.0 (SAS) and Prism, version 3 (GraphPad Software). Analysis of variance (ANOVA) was used to assess differences between groups. A P value of less than 0.05 was considered statistically significant. When ANOVA results were statistically significant, they were examined by Fisher's PLSD, or Dunnett's multiple comparison test, or Bonferroni-Dunn multiple comparisons post hoc test. Differences between *gad* mice and control mice were analyzed using the Mann-Whitney U test.

The authors thank Yuh Nung Jan and Hua-Shun Li for providing the immunohistochemistry methods; Yoshihiro Nakatani and Hidesato Ogawa for providing the retroviral expression system and immunoprecipitation methods; and Masako Shikama for the care and breeding of animals. This work was supported by Grants-in-Aid for Scientific Research from the Ministry of Health, Labour and Welfare of Japan, and Grants-in-Aid for Scientific Research from the Ministry of Education, Culture, Sports, Science and Technology of Japan.

References

Aoki, S., Su, Q., Li, H., Nishikawa, K., Ayukawa, K., Hara, Y., Namikawa, K., Kiryu-Seo, S., Kiyama, H. and Wada, K. (2002). Identification of an axotomy-induced glycosylated protein, AIGP1, possibly involved in cell death triggered by endoplasmic reticulum-Golgi stress. *J. Neurosci.* **22**, 10751-10760.

Arnaud, L., Ballif, B. A. and Cooper, J. A. (2003). Regulation of protein tyrosine kinase signaling by substrate degradation during brain development. *Mol. Cell. Biol.* **23**, 9293-9302.

Bock, H. H., Jossin, Y., May, P., Bergner, O. and Herz, J. (2004). Apolipoprotein E receptors are required for reelin-induced proteasomal degradation of the neuronal adaptor protein Disabled-1. *J. Biol. Chem.* **279**, 33471-33479.

Dickson, D. W., Schmidt, M. L., Lee, V. M., Zhao, M. L., Yen, S. H. and Trojanowski, J. Q. (1994). Immunoreactivity profile of hippocampal CA2/3 neurites in diffuse Lewy body disease. *Acta Neuropathol. (Berl.)* **87**, 269-276.

Fukuda, S., Kato, F., Tozuka, Y., Yamaguchi, M., Miyamoto, Y. and Hisatsune, T. (2003). Two distinct subpopulations of nestin-positive cells in adult mouse dentate gyrus. *J. Neurosci.* **23**, 9357-9366.

Hartfuss, E., Forster, E., Bock, H. H., Hack, M. A., Leprince, P., Luque, J. M., Herz, J., Frotscher, M. and Gotz, M. (2003). Reelin signaling directly affects radial glia morphology and biochemical maturation. *Development* **130**, 4597-4609.

Hashimoto, M. and Mikoshiba, K. (2004). Neuronal birthdate-specific gene transfer with adenoviral vectors. *J. Neurosci.* **24**, 286-296.

Kaufman, M. H., Brune, R. M., Davidson, D. R. and Baldock, R. A. (1998). Computer-generated three-dimensional reconstructions of serially sectioned mouse embryos. *J. Anat.* **193**, 323-336.

Kawauchi, T., Chihama, K., Nabeshima, Y. and Hoshino, M. (2003). The in vivo roles of STEF/Tiam1, Rac1 and JNK in cortical neuronal migration. *EMBO J.* **22**, 4190-4201.

Kwon, J., Kikuchi, T., Setsuie, R., Ishii, Y., Kyuwa, S. and Yoshikawa, Y. (2003). Characterization of the testis in congenitally ubiquitin carboxy-terminal hydrolase-1 (Uch-L1) defective (gad) mice. *Exp. Anim.* **52**, 1-9.

Larsen, C. N., Krantz, B. A. and Wilkinson, K. D. (1998). Substrate specificity of deubiquitinating enzymes: ubiquitin C-terminal hydrolases. *Biochemistry* **37**, 3358-3368.

Leroy, E., Boyer, R., Auburger, G., Leube, B., Ulm, G., Mezey, E., Harta, G., Brownstein, M. J., Jonnalagada, S., Chernova, T. et al. (1998). The ubiquitin pathway in Parkinson's disease. *Nature* **395**, 451-452.

Li, H. S., Wang, D., Shen, Q., Schonemann, M. D., Gorski, J. A., Jones, K. R., Temple, S., Jan, L. Y. and Jan, Y. N. (2003). Inactivation of Numb and Numblike in embryonic dorsal forebrain impairs neurogenesis and disrupts cortical morphogenesis. *Neuron* **40**, 1105-1118.

Liu, Y., Fallon, L., Lashuel, H. A., Liu, Z. and Lansbury, P. T., Jr (2002). The UCH-L1 gene encodes two opposing enzymatic activities that affect alpha-synuclein degradation and Parkinson's disease susceptibility. *Cell* **111**, 209-218.

Liu, Y., Lashuel, H. A., Choi, S., Xing, X., Case, A., Ni, J., Yeh, L. A., Cuny, G. D., Stein, R. L. and Lansbury, P. T., Jr (2003). Discovery of inhibitors that elucidate the role of UCH-L1 activity in the H1299 lung cancer cell line. *Chem. Biol.* **10**, 837-846.

Malatesta, P., Hartfuss, E. and Gotz, M. (2000). Isolation of radial glial cells by fluorescent-activated cell sorting reveals a neuronal lineage. *Development* **127**, 5253-5263.

Malatesta, P., Hack, M. A., Hartfuss, E., Kettenmann, H., Klinkert, W., Kirchhoff, F. and Gotz, M. (2003). Neuronal or glial progeny: regional differences in radial glia fate. *Neuron* **37**, 751-764.

McQuaid, S., McConnell, R., McMahon, J. and Herron, B. (1995). Microwave antigen retrieval for immunocytochemistry on formalin-fixed, paraffin-embedded post-mortem CNS tissue. *J. Pathol.* **176**, 207-216.

Nadarajah, B., Brunstrom, J. E., Grutzendler, J., Wong, R. O. and Pearlman, A. L. (2001). Two modes of radial migration in early development of the cerebral cortex. *Nat. Neurosci.* **4**, 143-150.

Nakashima, K., Yanagisawa, M., Arakawa, H., Kimura, N., Hisatsune, T., Kawabata, M., Miyazono, K. and Taga, T. (1999). Synergistic signaling in fetal brain by STAT3-Smad1 complex bridged by p300. *Science* **284**, 479-482.

Nishikawa, K., Li, H., Kawamura, R., Osaka, H., Wang, Y. L., Hara, Y., Hirokawa, T., Manago, Y., Amano, T., Noda, M. et al. (2003). Alterations of structure and

hydrolase activity of parkinsonism-associated human ubiquitin carboxyl-terminal hydrolase L1 variants. *Biochem. Biophys. Res. Commun.* 304, 176-183.

Noctor, S. C., Flint, A. C., Weissman, T. A., Dammerman, R. S. and Kriegstein, A. R. (2001). Neurons derived from radial glial cells establish radial units in neocortex. *Nature* 409, 714-720.

Noctor, S. C., Flint, A. C., Weissman, T. A., Wong, W. S., Clinton, B. K. and Kriegstein, A. R. (2002). Dividing precursor cells of the embryonic cortical ventricular zone have morphological and molecular characteristics of radial glia. *J. Neurosci.* 22, 3161-3173.

Noctor, S. C., Martinez-Cerdeno, V., Ivic, L. and Kriegstein, A. R. (2004). Cortical neurons arise in symmetric and asymmetric division zones and migrate through specific phases. *Nat. Neurosci.* 7, 136-144.

Ogawa, H., Ishiguro, K., Gaubatz, S., Livingston, D. M. and Nakatani, Y. (2002). A complex with chromatin modifiers that occupies E2F- and Myc-responsive genes in G0 cells. *Science* 296, 1132-1136.

Osaka, H., Wang, Y. L., Takada, K., Takizawa, S., Setsuie, R., Li, H., Sato, Y., Nishikawa, K., Sun, Y. J., Sakurai, M. et al. (2003). Ubiquitin carboxy-terminal hydrolase L1 binds to and stabilizes monoubiquitin in neuron. *Hum. Mol. Genet.* 12, 1945-1958.

Patrick, G. N., Zhou, P., Kwon, Y. T., Howley, P. M. and Tsai, L. H. (1998). p35, the neuronal-specific activator of cyclin-dependent kinase 5 (Cdk5) is degraded by the ubiquitin-proteasome pathway. *J. Biol. Chem.* 273, 24057-24064.

Qian, X., Goderie, S. K., Shen, Q., Stern, J. H. and Temple, S. (1998). Intrinsic programs of patterned cell lineages in isolated vertebrate CNS ventricular zone cells. *Development* 125, 3143-3152.

Qian, X., Shen, Q., Goderie, S. K., He, W., Capela, A., Davis, A. A. and Temple, S. (2000). Timing of CNS cell generation: a programmed sequence of neuron and glial cell production from isolated murine cortical stem cells. *Neuron* 28, 69-80.

Qiu, L., Joazeiro, C., Fang, N., Wang, H. Y., Elly, C., Altman, Y., Fang, D., Hunter, T. and Liu, Y. C. (2000). Recognition and ubiquitination of Notch by Itch, a hect-type E3 ubiquitin ligase. *J. Biol. Chem.* 275, 35734-35737.

Rice, D. S. and Curran, T. (2001). Role of the reelin signaling pathway in central nervous system development. *Annu. Rev. Neurosci.* 24, 1005-1039.

Roegiers, F. and Jan, Y. N. (2004). Asymmetric cell division. *Curr. Opin. Cell Biol.* 16, 195-205.

Saigoh, K., Wang, Y. L., Suh, J. G., Yamanishi, T., Sakai, Y., Kiyosawa, H., Harada, T., Ichihara, N., Wakana, S., Kikuchi, T. et al. (1999). Intragenic deletion in the gene encoding ubiquitin carboxy-terminal hydrolase in gad mice. *Nat. Genet.* 23, 47-51.

Satoh, J. and Kuroda, Y. (2001). A polymorphic variation of serine to tyrosine at codon 18 in the ubiquitin C-terminal hydrolase-L1 gene is associated with a reduced risk of sporadic Parkinson's disease in a Japanese population. *J. Neurol. Sci.* 189, 113-117.

Sauvageot, C. M. and Stiles, C. D. (2002). Molecular mechanisms controlling cortical gliogenesis. *Curr. Opin. Neurobiol.* 12, 244-249.

Schofield, J. N., Day, I. N., Thompson, R. J. and Edwards, Y. H. (1995). PGP9.5, a ubiquitin C-terminal hydrolase; pattern of mRNA and protein expression during neural development in the mouse. *Brain Res. Dev. Brain Res.* 85, 229-238.

Sekiguchi, S., Yoshikawa, Y., Tanaka, S., Kwon, J., Ishii, Y., Kyuwa, S., Wada, K., Nakamura, S. and Takahashi, K. (2003). Immunohistochemical analysis of protein gene product 9.5, a ubiquitin carboxyl-terminal hydrolase, during placental and embryonic development in the mouse. *Exp. Anim.* 52, 365-369.

Shen, Q., Qian, X., Capela, A. and Temple, S. (1998). Stem cells in the embryonic cerebral cortex: their role in histogenesis and patterning. *J. Neurobiol.* 36, 162-174.

Sullivan, M. L. and Vierstra, R. D. (1993). Formation of a stable adduct between ubiquitin and the Arabidopsis ubiquitin-conjugating enzyme, AtUBC1+. *J. Biol. Chem.* 268, 8777-8780.

Tabata, H. and Nakajima, K. (2003). Multipolar migration: the third mode of radial neuronal migration in the developing cerebral cortex. *J. Neurosci.* 23, 9996-10001.

Temple, S. (2001). The development of neural stem cells. *Nature* 414, 112-117.

Weissman, A. M. (2001). Themes and variations on ubiquitylation. *Nat. Rev. Mol. Cell. Biol.* 2, 169-178.

Wilkinson, K. D., Lee, K. M., Deshpande, S., Duerksen-Hughes, P., Boss, J. M. and Pohl, J. (1989). The neuron-specific protein PGP 9.5 is a ubiquitin carboxyl-terminal hydrolase. *Science* 246, 670-673.

Zhong, W., Feder, J. N., Jiang, M. M., Jan, L. Y. and Jan, Y. N. (1996). Asymmetric localization of a mammalian numb homolog during mouse cortical neurogenesis. *Neuron* 17, 43-53.

Zhong, W., Jiang, M. M., Weinmaster, G., Jan, L. Y. and Jan, Y. N. (1997). Differential expression of mammalian Numb, Numblike and Notch1 suggests distinct roles during mouse cortical neurogenesis. *Development* 124, 1887-1897.